Geophysical Journal International

Advancing Astronomy and Geophysics

Geophys. J. Int. (2021) 227, 1228–1245 Advance Access publication 2021 July 15 GJI Geomagnetism, Rock Magnetism and Palaeomagnetism https://doi.org/10.1093/gji/ggab274

Large-scale balances and asymptotic scaling behaviour in spherical dynamos

Michael A. Calkins[®], Ryan J. Orvedahl^{®2} and Nicholas A. Featherstone^{®3}

- ¹Department of Physics, University of Colorado, Boulder, CO 80309, USA, E-mail: michael.calkins@colorado.edu
- ²Department of Astrophysical and Planetary Sciences, University of Colorado, Boulder, CO 80309, USA

Accepted 2021 July 8. Received 2021 March 25; in original form 2021 June 21

SUMMARY

The large-scale dynamics of convection-driven dynamos in a spherical shell, as relevant to the geodynamo, is analysed with numerical simulation data and asymptotic theory. An attempt is made to determine the asymptotic size (with the small parameter being the Ekman number, Ek) of the forces, and the associated velocity and magnetic fields. In agreement with previous work, the leading order mean force balance is shown to be thermal wind (Coriolis, pressure gradient and buoyancy) in the meridional plane and Coriolis-Lorentz in the zonal direction. The Lorentz force is observed to be weaker than the mean buoyancy force across a range of Ek and thermal forcing; the relative difference in these forces appears to be $O(Ek^{1/6})$ within the parameter space investigated. We find that the thermal wind balance requires that the mean zonal velocity scales as $O(Ek^{-1/3})$, whereas the meridional circulation is asymptotically smaller by a factor of $O(Ek^{1/6})$. The mean temperature equation shows a balance between thermal diffusion and the divergence of the convective heat flux, indicating the presence of a mean temperature length scale of size $O(Ek^{1/6})$. Neither the mean nor the fluctuating magnetic field show a strong dependence on the Ekman number, though the simulation data shows evidence of a mean magnetic field length scale of size $O(Ek^{1/6})$. A consequence of the asymptotic ordering of the forces is that Taylor's constraint is satisfied to accuracy $O(Ek^{1/6})$, despite the absence of a leading-order magnetostrophic balance. Further consequences of the force balance are discussed with respect to the large-scale flows thought to be important for the geodynamo.

Key words: Core; Dynamo: theories and simulations; Numerical modelling; Planetary interiors.

1 INTRODUCTION

The geomagnetic field has existed for at least 3.5 billion years, and possibly as long as 4.2 billion years (Tarduno *et al.* 2015). It is known that the geomagnetic field is characterized by a broad range of spatiotemporal scales. Temporal changes in the field that are thought to be directly linked to interior dynamics range from the 10⁵ yr timescale for magnetic polarity reversals (e.g. Amit *et al.* 2010) to years for large scale oscillations (Gillet *et al.* 2015). The resulting flow patterns in the outer core inferred from secular variation exhibit a rich structure (Hulot *et al.* 2002; Amit & Olson 2004; Gillet *et al.* 2015; Livermore *et al.* 2017). Understanding the origin of these different spatiotemporal scales and their subsequent evolution requires knowledge of the predominant forces within the core. It is generally accepted that the Coriolis force is a key ingredient for the generation of the geomagnetic field in the core, but the relative sizes of other forces in the core is still debated (see e.g.

Aurnou & King 2017). One view is that the core dynamics are dominated by a four-way, magnetostrophic balance in which the Coriolis, pressure gradient, buoyancy and Lorentz forces are all of comparable magnitude (e.g. Roberts & King 2013). An alternative view is that the core is characterized by a geostrophic balance in which only the Coriolis and pressure gradient forces balance, and the Lorentz force would contribute only as a perturbation to the primary geostrophic balance (Calkins 2018). Here we use data from numerical dynamo models, along with asymptotic analysis of the governing equations to interrogate the force balance in more detail. Recent numerical simulations indicate that a leading order geostrophic force balance is present on what we refer to as the smallscale motions (Soderlund et al. 2012; Yadav et al. 2016; Aubert et al. 2017; Schaeffer et al. 2017; Schwaiger et al. 2021). In contrast to these recent studies, we focus on the dynamics of the large-scale motions, which can be simply defined as the longitudinally averaged, or axisymmetric motions.

³ Southwest Research Institute, 1050 Walnut Street Suite 400, Boulder, CO 80302, USA

No direct observations of the core are currently possible. Instead, insight into core dynamics is obtained from temporal variations of the geomagnetic field. These observations suggest a typical flow speed in the core is $U \sim 10^{-4} \text{ m s}^{-1}$ (Roberts & King 2013). Coupled with physical properties of the core obtained from laboratory experiments and simulations (e.g. Pozzo et al. 2013), this value provides vital clues to the inner workings of the core by enabling estimates of important non-dimensional parameters describing the dynamics of the core. In particular, the relative size of inertia compared to the Coriolis force is quantified by the Rossby number Ro = $U/(\Omega d)$, where Ω and d are the rotation rate and depth of the outer core, respectively. The relative size of the viscous force to the Coriolis force is measured by the Ekman number $Ek = \nu/(\Omega d^2)$ where ν is the kinematic viscosity of the core. Estimates suggest values of Ro $\approx 10^{-6}$ and Ek $\approx 10^{-15}$ for the core (King et al. 2010). The Elsasser number $\Lambda = \sigma B^2/(\rho \Omega)$ (where σ is electrical conductivity, B is the typical magnetic field strength and ρ is the density) characterizes the relative size of the Lorentz and Coriolis forces; studies suggest $\Lambda \approx 1$ in the core (see e.g. Stevenson 2003; King et al. 2010). The small magnitude of the Rossby and Ekman numbers suggest that inertia and viscosity are small on the global scale of the core, whereas $\Lambda \approx 1$ suggests that the Lorentz force and Coriolis force are comparable in magnitude. However, these estimates must be interpreted carefully as it is unclear what scales of motion are observed in secular variation studies.

The small values of the Rossby and Ekman numbers indicate that the Earth's core operates in a rapidly rotating regime (Aurnou et al. 2015). Spatial scale separation is an intrinsic property of rapidly rotating flows, and perturbation theory has exploited this scale separation successfully to describe the asymptotic behaviour of the linear dynamics of spherical convection (Roberts 1968; Busse 1970; Soward 1977; Jones et al. 2000; Dormy et al. 2004). These tools have also been applied to both the linear (Chandrasekhar 1961) and nonlinear dynamics (Julien et al. 1998) of the plane layer geometry in the asymptotic limit of small Ekman number. The plane layer theory is significantly simpler in comparison to the spherical theory since only two dominant length scales (the depth d, and the small $d \to k^{1/3}$ convective length scale) are present in the system. In contrast, the sphere contains a multitude of different length scales, including the system scale d, the convective radial envelope scale $d \to k^{1/6}$, and the convective length scale $d \to k^{1/3}$ (Jones et al. 2000). Linear and nonlinear asymptotic theories for the sphere must account for all of these scales. Here we attempt to use elements of asymptotic theory to better understand the large-scale dynamics of rotating spherical dynamos. Identifying asymptotic behaviour in models is an important step when comparing modelling results to natural systems such as the Earth's core, and may help identify pathways for the development of nonlinear, multiscale asymptotic models for the spherical geometry (cf. Calkins et al. 2013, 2015).

When inertia and viscosity are neglected in the momentum equation, Taylor (1963) showed that the component of the Lorentz torque aligned along the rotation axis must vanish. This condition is referred to as 'Taylor's constraint' and is expressed mathematically as

$$\int \widehat{\boldsymbol{\phi}} \cdot \left(\overline{\boldsymbol{J} \times \boldsymbol{B}} \right) \, \mathrm{d}z = 0, \tag{1}$$

where $\widehat{\phi} \cdot (\overline{J \times B})$ is the zonal component of the Lorentz force and z is the cylindrical coordinate aligned along the rotation axis. Flows that obey this constraint are said to be in a 'Taylor state'. Since real fluids experience both viscous and ohmic dissipation, and undergo

acceleration, Taylor's constraint is expected to be satisfied only in an approximate sense. Deviations from a Taylor state lead to a form of axisymmetric Alfvén waves known as torsional oscillations (Braginsky 1970).

Recent studies have been devoted to finding exact Taylor states (see e.g. Livermore *et al.* 2016; Hardy *et al.* 2018), some of which include the use of mean-field electrodynamics to produce kinematic dynamos that satisfy leading-order magnetostrophic balance (Wu & Roberts 2015; Li *et al.* 2018). However, numerical dynamo simulations do not observe a leading-order magnetostrophic balance (Yadav *et al.* 2016; Aubert *et al.* 2017). One argument is that such simulations are dominated by viscosity, and the simulated dynamics are therefore in a parameter regime that is not representative of the geodynamo (Wu & Roberts 2015). However, the available data does not support this view in the sense that simulations do not show any sudden changes in dynamic behaviour as the Ekman number is reduced; this asymptotically 'smooth' behaviour is confirmed in the present work and argued from an asymptotic standpoint.

There is evidence that axially invariant torsional oscillations are present in geomagnetic field observations, and have been observed in numerical simulations (e.g., Gillet et al. 2010; Roberts & Aurnou 2012; Schaeffer et al. 2017). Not surprisingly, the relative amplitude of such flows is larger when viscous effects are weaker, and more recent simulations using smaller values of the Ekman number therefore observe clear torsional oscillation signals (Schaeffer et al. 2017). The work of Wicht & Christensen (2010) examined how the relative sizes of the forces in numerical dynamo simulations affect torsional oscillations. In particular, by decomposing the velocity field into toroidal and poloidal components, Wicht & Christensen (2010) find that the toroidal balance is dominated by the Lorentz and Coriolis forces, but this component is weaker than the forces present in the poloidal balance. Here, we provide an argument for why this ordering occurs, and we attempt to connect this observation to Taylor's constraint.

Although several recent numerical studies have analysed the force balances observed in numerical dynamo simulations (e.g. Soderlund et al. 2012; Yadav et al. 2016; Aubert et al. 2017; Schaeffer et al. 2017), the majority of these investigations have focused on the small-scale force balances, or did not distinguish between the relevant length scales. However, asymptotic models show that distinct balances can be present on different spatiotemporal scales (Phillips 1963; Julien & Knobloch 2007; Grooms et al. 2011; Calkins et al. 2015). Previous work has shown that the small-scale force balance in rotating spherical dynamo models is characterized by a leading order geostrophic force balance, and a secondary (i.e. higher order) magnetostrophic balance (Yadav et al. 2016). In contrast, Aubert (2005) showed that the large-scale dynamics observed in dynamo simulations are well-described by a thermal wind balance in meridional planes, whereas the azimuthal force balance is dominated by a balance between the mean Coriolis force and the mean Lorentz force. Recent work has confirmed that this azimuthal force balance persists at lower Ekman numbers and is nearly scale independent (Sheyko et al. 2018).

Our primary goal with the present work is to further investigate the large scale balances in spherical dynamos using asymptotic theory, in order to provide estimates for the relative sizes (in terms of the Ekman number) of the forces and associated quantities. Our results suggest that rapidly rotating spherical dynamos satisfy Taylor's constraint up to order $O(\text{Ek}^{1/6})$, despite not being characterized by a magnetostrophic balance. Whereas the analysis of Braginsky (1976) neglected the influence of buoyancy, here we show that its inclusion indicates that axially invariant torsional

oscillations are only a single component of a richer set of dynamics. We also highlight that the large-scale balance, in particular the Coriolis-Lorentz balance in the zonal direction, is consistent with the so-called Malkus-Proctor scenario (Malkus & Proctor 1975) in which a large-scale magnetic field is saturated by the generation of a large-scale flow. However, we emphasize that this large-scale flow consists of the meridional circulation, which is observed (and perhaps expected) to be asymptotically weaker than the corresponding mean zonal flow. In Section 2, we present the governing equations, non-dimensional control parameters and mean-fluctuating decomposition; in Section 3 we present arguments for the asymptotic sizes of the various forces; in Section 4 we compare with numerical simulations. A discussion of the implications for Taylor's constraint is given in Section 5 and conclusions are given in Section 6.

2 GOVERNING EQUATIONS

We consider an Oberbeck–Boussinesq fluid with density ρ , kinematic viscosity ν , magnetic diffusivity η , thermal expansion coefficient α and thermal diffusivity κ . The geometry consists of a rotating spherical shell of inner and outer radii r_i and r_o , respectively, so that the depth of the fluid is $d = r_0 - r_i$. In this work the non-dimensional aspect ratio $\chi = r_i/r_o = 0.35$ is fixed in all simulations presented. The rotation and gravity vectors are given by $\Omega = \Omega \hat{z}$ and $g = -g_o r/r_o$, where \hat{z} is a Cartesian basis vector, r is the position vector and g_o is the gravitational acceleration at the outer boundary. We non-dimensionalize the governing equations with the depth d, large scale viscous diffusion timescale d^2/v , magnetic field scale $\mathcal{B}^2 = \mu_0 \rho \eta \Omega$ and pressure scale $\mathcal{P} = \rho \nu \Omega$; the equations become

$$\partial_{t} \boldsymbol{u} + \boldsymbol{u} \cdot \nabla \boldsymbol{u} + \frac{2}{Ek} \widehat{\boldsymbol{z}} \times \boldsymbol{u} = -\frac{1}{Ek} \nabla P + \frac{Ra}{Pr} \frac{\boldsymbol{r}}{r_{o}} T + \frac{1}{PmEk} \boldsymbol{J} \times \boldsymbol{B} + \nabla^{2} \boldsymbol{u},$$
 (2)

$$\partial_t \mathbf{B} = \nabla \mathbf{x} \left(\mathbf{u} \mathbf{x} \mathbf{B} \right) + \frac{1}{\text{Pm}} \nabla^2 \mathbf{B}, \tag{3}$$

$$\partial_t T + \boldsymbol{u} \cdot \nabla T = \frac{1}{\text{Pr}} \nabla^2 T, \tag{4}$$

$$\nabla \cdot \boldsymbol{u} = \nabla \cdot \boldsymbol{B} = 0, \tag{5}$$

where the flow variables are the velocity $\mathbf{u} = (u_r, u_\theta, u_\phi)$, pressure P, temperature T, magnetic field $\mathbf{B} = (B_r, B_\theta, B_\phi)$ and current density $J = \nabla \times B$.

The non-dimensional control parameters are the Ekman, Rayleigh, Prandtl and magnetic Prandtl numbers defined by, respectively,

$$Ek = \frac{v}{\Omega d^2}, \quad Ra = \frac{g_o \alpha \Delta T^* d^3}{v \kappa}, \quad Pr = \frac{v}{\kappa}, \quad Pm = \frac{v}{\eta}, \quad (6)$$

where ΔT^* is the dimensional temperature difference between the inner and outer boundaries. The flow speed is measured in units of the large-scale Reynolds number

$$Re = \frac{Ud}{V}.$$
 (7)

The boundary conditions used in the present work are identical for all simulations. We use impenetrable, no-slip boundary conditions for the velocity field,

$$\boldsymbol{u}\left(r_{o}\right) = \boldsymbol{u}\left(r_{i}\right) = 0. \tag{8}$$

The heat equation is solved with isothermal boundary conditions such that

$$T(r_i) = 1$$
 and $T(r_o) = 0$. (9)

Finally, electrically insulating boundary conditions are applied such that J = 0 at both the inner and outer boundaries.

The equations are discretized in physical space utilizing a spherical harmonic decomposition in colatitude and longitude (θ, ϕ) , and Chebyshev polynomials in radius, r. The time-stepping algorithm is a 2nd order semi-implicit Adams-Bashforth/Crank-Nicolson method in which all non-linear terms and the Coriolis force are treated explicitly, and the remaining linear terms are treated implicitly. A pseudospectral approach is used where the linear terms are computed in spectral space and the non-linear terms are computed in physical space. Further details of the numerical method and the parallelization are found in Featherstone & Hindman (2016) and Matsui et al. (2016).

2.1 Decomposition

For the analysis we decompose all of the dependent variables into mean (large-scale) and fluctuating (small-scale) components according to

$$f = \overline{f} + f', \tag{10}$$

where f is a generic dependent variable. We note that in the analysis that follows there is no a priori requirement on the relative sizes of \overline{f} and f. The definition of the mean component, and therefore also of the fluctuating component, is arbitrary since it is not generally known a priori how one distinguishes 'large-scale' versus 'smallscale' dynamics. For simplicity we use an azimuthal average,

$$\overline{f} = \frac{1}{2\pi} \int_{0}^{2\pi} f \, \mathrm{d}\phi, \qquad \overline{f'} \equiv 0. \tag{11}$$

Substituting the above decomposition for each of the dependent variables into the governing equations, averaging in longitude and subtracting the resulting mean equations from the total equations yields two sets of coupled equations. Although we restrict the present analysis to the mean equations, we show the fluctuating equations for completeness. The mean equations become

$$\partial_{t}\overline{\boldsymbol{u}} = -\overline{\boldsymbol{u}\cdot\nabla\boldsymbol{u}} - \frac{2}{Ek}\widehat{\boldsymbol{z}}\times\overline{\boldsymbol{u}} - \frac{1}{Ek}\nabla\overline{P} + \nabla^{2}\overline{\boldsymbol{u}}$$
$$+ \frac{1}{PmFk}\overline{\boldsymbol{J}\times\boldsymbol{B}} + \frac{Ra}{Pr}\frac{\boldsymbol{r}}{r}. \overline{T}, \tag{12}$$

$$\partial_t \overline{T} + \overline{u} \cdot \nabla \overline{T} + \nabla \cdot \left(\overline{u'T'} \right) = \frac{1}{\Pr} \nabla^2 \overline{T},$$
 (13)

$$\partial_{t}\overline{B} = \nabla \times (\overline{u} \times \overline{B}) + \nabla \times \overline{\mathcal{E}} + \frac{1}{Pm} \nabla^{2} \overline{B}, \tag{14}$$

$$\nabla \cdot \overline{\boldsymbol{u}} = 0, \qquad \nabla \cdot \overline{\boldsymbol{B}} = 0, \tag{15}$$

where the emf is defined by

$$\overline{\mathcal{E}} = \overline{u' \times B'}. \tag{16}$$

The corresponding fluctuating equations are given by

$$\partial_{t} \mathbf{u}' = -\mathbf{u} \cdot \nabla \mathbf{u} + \overline{\mathbf{u} \cdot \nabla \mathbf{u}} - \frac{2}{Ek} \widehat{\mathbf{z}} \times \mathbf{u}' - \frac{1}{Ek} \nabla P' + \nabla^{2} \mathbf{u}' + \frac{1}{PmEk} \left(\mathbf{J} \times \mathbf{B} - \overline{\mathbf{J} \times \mathbf{B}} \right) + \frac{Ra}{Pr} \frac{\mathbf{r}}{r_{o}} T',$$
(17)

$$\partial_t T' + \boldsymbol{u} \cdot \nabla T' + \boldsymbol{u}' \cdot \nabla \overline{T} - \overline{\boldsymbol{u}' \cdot \nabla T'} = \frac{1}{P_r} \nabla^2 T', \tag{18}$$

$$\partial_t \mathbf{B}' = \nabla \times \left(\overline{\mathbf{u}} \times \mathbf{B}' \right) + \nabla \times \left(\mathbf{u}' \times \overline{\mathbf{B}} \right) + \nabla \times \mathbf{G} + \frac{1}{\mathsf{Pm}} \nabla^2 \mathbf{B}', \quad (19)$$

$$\nabla \cdot \boldsymbol{u}' = 0, \qquad \nabla \cdot \boldsymbol{B}' = 0, \tag{20}$$

where

$$G = u' \times B' - \overline{\mathcal{E}}. \tag{21}$$

For the momentum equations we have pulled all terms, with the exception of the time derivative of the velocity, to the right-hand side of the equations. We refer to time derivatives of the various velocity vectors $(\partial_t \mathbf{u})$, and the decomposed counterparts $\partial_t \overline{\mathbf{u}}$ and $\partial_t \mathbf{u}'$) as inertia. The advective non-linearities, that is those terms arising from either the mean or fluctuating components of the term $\mathbf{u} \cdot \nabla \mathbf{u}$, are referred to as advection. For shorthand, we can then write each momentum equation as

$$\partial_t \mathbf{u} = \mathbf{F}_a + \mathbf{F}_c + \mathbf{F}_p + \mathbf{F}_v + \mathbf{F}_l + \mathbf{F}_h, \tag{22}$$

$$\partial_t \overline{\boldsymbol{u}} = \overline{\boldsymbol{F}}_a + \overline{\boldsymbol{F}}_c + \overline{\boldsymbol{F}}_p + \overline{\boldsymbol{F}}_v + \overline{\boldsymbol{F}}_l + \overline{\boldsymbol{F}}_b, \tag{23}$$

$$\partial_t \mathbf{u}' = \mathbf{F}_a' + \mathbf{F}_c' + \mathbf{F}_n' + \mathbf{F}_n' + \mathbf{F}_h' + \mathbf{F}_h', \tag{24}$$

where the various subscripts denote advection ('a'), Coriolis force ('c'), pressure gradient force ('p'), viscous force ('v'), Lorentz force ('l') and buoyancy force ('b'). In terms of the Reynolds decomposition, the non-linear terms are then

$$\overline{F}_a = -\overline{u} \cdot \nabla \overline{u} - \overline{u' \cdot \nabla u'}, \tag{25}$$

$$\overline{F}_l = \overline{J} \times \overline{B} + \overline{J' \times B'}, \tag{26}$$

$$F'_{a} = -\overline{u} \cdot \nabla u' - u' \cdot \nabla \overline{u} - u' \cdot \nabla u' + \overline{u' \cdot \nabla u'}, \tag{27}$$

$$F'_{I} = (\overline{J} \times B') + (J' \times \overline{B}) + (J' \times B') - (\overline{J' \times B'}). \tag{28}$$

In what follows, we subtract the spherically symmetric components of the forces (defined by spherical harmonic degree $\ell=0$) from the radial component of the mean momentum equation since they represent hydrostatic balance and play no dynamic role.

3 BALANCES: ASYMPTOTIC SCALING ARGUMENTS

Previous numerical studies have shown that the large-scale force balance in rapidly rotating spherical dynamos consists of a thermal-wind balance in the meridional (r, θ) plane,

$$\frac{2}{\operatorname{Ek}}\widehat{\mathbf{z}}\times\overline{\mathbf{u}}\approx -\frac{1}{\operatorname{Ek}}\nabla\overline{P} + \frac{\operatorname{Ra}}{\operatorname{Pr}}\overline{T}\frac{\mathbf{r}}{r_{\star}},\tag{29}$$

and a mean Coriolis–Lorentz force balance in the zonal (longitudinal, ϕ) direction (e.g. Aubert 2005),

$$\frac{2}{\text{Ek}}\overline{u}_{s} \approx \frac{1}{\text{EkPm}} \left(\overline{\boldsymbol{J} \times \boldsymbol{B}} \right)_{\phi}, \tag{30}$$

where the mean cylindrical radial component of the velocity is defined as

$$\overline{u}_s = \cos\theta \, \overline{u}_\theta + \sin\theta \, \overline{u}_r. \tag{31}$$

For brevity we refer to \overline{u}_s as 'meridional circulation' since it depends on both of the meridional components of the mean velocity vector. Since the Lorentz force enters only a single component of the leading-order force balance, we refer to this force balance as

semi-magnetostrophic (MS). Our goal is to determine the asymptotic size of each term in the semi-MS force balance. This process constitutes one of the differences between this work and that of Taylor (1963), where the asymptotic scaling of the forces was not discussed. Rather, Taylor (1963) neglected the effects of viscosity and inertia at the outset and did not explicitly separate large and small scale quantities, whereas we want to understand how the various forces scale as the physical parameters are made more core-like. Not only is performing such an analysis important for theoretical understanding, it also provides a method for relating the output of numerical models to natural systems.

Here we assume that the small magnitude of the Ekman number controls the dynamics of rapidly rotating systems such as the Earth's outer core. Therefore, we choose our small parameter as

$$\epsilon \equiv Ek^{1/3}. \tag{32}$$

Hereafter, when the order of a quantity is specified it refers to its asymptotic size with respect to ϵ , or equivalently the Ekman number. Convection occurs only when the Rayleigh number exceeds a critical value, Ra_{crit}, which scales as Ra_{crit} = $O(\epsilon^{-4})$ (Chandrasekhar 1961; Roberts 1968; Busse 1970). Thus, we use a reduced (asymptotically scaled) Rayleigh number (see e.g. Julien *et al.* 1998; Jones *et al.* 2000) defined as

$$\widetilde{Ra} \equiv \epsilon^4 Ra = O(1). \tag{33}$$

The assumption on the scaling of the Rayleigh number is valid so long as the dynamo is driven by rapidly rotating convection; this is automatically satisfied in any small-Ekman number dynamo simulation that has a supercritical Rayleigh number. All other non-dimensional parameters are assumed to be order one in the sense that they do not scale with the Ekman number. The influence of small values of Pm is beyond the scope of the present work since we focus on regimes of Pm that are currently accessible to numerical simulations [for a discussion of the influence of various limits of Pm see Calkins (2018) and references therein]. Although we are assuming a small parameter that is based on the viscous length scale, as represented by eq. (32), this does not imply that the viscous force enters the leading order force balance (cf. Jones et al. 2000; Julien et al. 1998).

With the above definitions, the mean buoyancy force can be written as

$$\overline{F}_{b} = \epsilon^{-4} \frac{\widetilde{Ra}}{\operatorname{Pr}} \frac{r}{r_{o}} \overline{T}.$$
(34)

The geometric factor is order unity, that is $r/r_o = O(1)$. The asymptotic size of the mean temperature is controlled by the thermal boundary conditions and, since such conditions do not depend on the Ekman number, we assume

$$\overline{T} = O(1) \quad \Rightarrow \quad |\overline{F}_{b}| = O(\epsilon^{-4}).$$
 (35)

The above assumption is tested with the numerical data. The mean Coriolis force is given by

$$\overline{F}_{c} = \begin{pmatrix} \overline{F}_{c,r} \\ \overline{F}_{c,\theta} \\ \overline{F}_{c,\phi} \end{pmatrix} = \frac{2}{\epsilon^{3}} \begin{pmatrix} \overline{u}_{\phi} \sin \theta \\ \overline{u}_{\phi} \cos \theta \\ -\overline{u}_{s} \end{pmatrix}, \tag{36}$$

thus the meridional components scale as $O\left(\epsilon^{-3}\overline{u}_{\phi}\right)$ and the zonal component scales as $O\left(\epsilon^{-3}\overline{u}_{s}\right)$. For a thermal wind balance to occur, the radial components must balance such that

$$\overline{F}_{b,r} \sim \overline{F}_{c,r} \qquad \Rightarrow \qquad \overline{u}_{\phi} = O\left(\epsilon^{3}\overline{F}_{b,r}\right) = O\left(\epsilon^{-1}\right).$$
 (37)

This scaling suggests that the zonal flow becomes increasingly strong as the Ekman number is decreased. The asymptotic scaling for the mean zonal flow is identical to the scaling of the small-scale velocity field in rapidly rotating convection in both spherical and Cartesian geometries (Julien *et al.* 1998; Jones *et al.* 2000). The pressure gradient must also balance with the buoyancy force so that

$$\overline{F}_{\mathrm{p},r} \sim \overline{F}_{\mathrm{b},r} = O\left(\epsilon^{-4}\right).$$
 (38)

The corresponding scalings for the θ -component are

$$\overline{F}_{\mathbf{p},\theta} \sim \overline{F}_{\mathbf{c},\theta} = O\left(\epsilon^{-4}\right).$$
 (39)

We note that the thermal wind balance seems to provide a direct scaling for the zonal velocity in terms of the Ekman, Rayleigh and Prandtl numbers; balancing the radial components of the mean Coriolis force and the mean buoyancy force yields

$$\overline{u}_{\phi} \sim \frac{\text{EkRa}}{\text{Pr}},$$
 (40)

where again the mean temperature is assumed to be order one. Because neither the buoyancy force nor the Coriolis force involve diffusion coefficients, the above scaling might be referred to as 'diffusion-free' given that both the kinematic viscosity and the thermal diffusivity cancel since the velocity has non-dimensional units of large scale Reynolds number and therefore scales as v^{-1} . For instance, the above scaling has been suggested by Guervilly et al. (2019), though they used different scaling arguments. Recent plane layer simulations of small Rossby number convection find that such a scaling may be valid over a limited range in Rayleigh number yet the formation of large-scale vortices seems to influence the observed scaling (Maffei et al. 2021). However, we note that the interpretation of eq. (40) as diffusion-free is incorrect because the Rayleigh number scales as Ra \sim Ek^{-4/3}, which leads to the $\overline{u}_{\phi} \sim$ Ek^{-1/3} scaling derived from relation (37), implying that the zonal flow does indeed scale with the Ekman number. Though the complete scaling behaviour of the zonal velocity (in terms of its dependence on the combination of all input parameters such as the Ekman, Rayleigh and Prandtl numbers) is of significant interest, we leave the detailed investigation of this matter for a future study; in the present work we focus primarily on the Ekman number dependence.

The zonal force balance between the Coriolis and Lorentz forces requires

$$\left(\overline{J \times B}\right)_{\phi} = O\left(\overline{u}_{s}\right),\tag{41}$$

where, again, we assume that Pm = O(1). In general, the Lorentz force provides the non-linearity that is required to arrest any possible exponential growth in the magnetic field. The Coriolis-Lorentz force balance shown above provides this non-linearity in the mean magnetic field, and therefore provides a constraint on the size of the mean magnetic field, provided that a corresponding constraint on the size of \overline{u}_s can be obtained. Given that the zonal Coriolis–Lorentz balance is the first appearance of the mean Lorentz force (in terms of asymptotic size) in the governing equations, this suggests that these large-scale dynamos are saturated by the so-called Malkus-Proctor scenario (Malkus & Proctor 1975): the mean magnetic field becomes saturated through the formation of a mean flow, which in this case is the meridional circulation. We also note that the above balance automatically implies that an Elsasser number based on the zonal components of the Coriolis and Lorentz, denoted by Λ_{ϕ} , is order unity, that is $\Lambda_{\phi} = O(1)$, despite the fact that the Lorentz force does not enter the leading order force balance (cf. Calkins 2018).

From a dynamic perspective, we expect that the meridional circulation is much weaker than the zonal flow such that $O\left(\overline{u}_s\right) \ll O\left(\overline{u}_\phi\right)$. In the simulations discussed here the meridional circulation is roughly an order of magnitude smaller than the mean zonal flow. Therefore, we expect the meridional dynamics will be asymptotically decoupled from the mean zonal dynamics in the sense that the leading-order components of the forces will be of different asymptotic order. We note that the continuity equation provides no constraint on the size of \overline{u}_s since both components of the meridional circulation are assumed to scale with ϵ in the same manner and are assumed to vary on similar length scales.

A constraint on the scaling of the meridional circulation can be found by comparing the Lorentz force to the buoyancy force. First, we assume that the individual components of the Lorentz force are all of comparable size,

$$(\overline{J \times B})_r \approx (\overline{J \times B})_\theta \approx (\overline{J \times B})_\phi.$$
 (42)

For the semi-MS force balance to occur, the Lorentz force must be weaker than the buoyancy force.

$$\frac{1}{\mathsf{PmFk}} \left(\overline{\boldsymbol{J} \times \boldsymbol{B}} \right)_r \ll \overline{F}_{\mathsf{b},r}, \qquad \Rightarrow \qquad \left(\overline{\boldsymbol{J} \times \boldsymbol{B}} \right)_r = o\left(\epsilon^{-1} \right), \quad (43)$$

where $o(\cdot)$ indicates little-o notation. Little-o notation describes an asymptotic inequality, that is f = o(g) indicates that f is asymptotically smaller than g, where f and g are arbitrary functions. Since the Lorentz force components are all of comparable magnitude, the above constraint can also be written as

$$\left(\overline{J \times B}\right)_{\phi} = o\left(\epsilon^{-1}\right). \tag{44}$$

Then, using the Coriolis–Lorentz force balance in the zonal component of the mean momentum equation, we can place a constraint on the asymptotic size of the meridional circulation as

$$\overline{u}_s = o\left(\epsilon^{-1}\right). \tag{45}$$

We attempt to further constrain the asymptotic size of the meridional circulation by examining dominant balances in the mean temperature equation, rewritten here as

$$\partial_t \overline{T} + \overline{u} \cdot \nabla \overline{T} + \nabla \cdot \left(\overline{u'T'} \right) = \frac{1}{\mathbf{p_r}} \nabla^2 \overline{T}. \tag{46}$$

Such dominant balances are assumed possible from the outset and justified a posteriori. In what follows we denote all mean length scales as $\overline{\ell}$. A subscript is used to specify the quantity that a given length scale characterizes, such that $\overline{\ell}_T$ denotes the length scale for the mean temperature. We further assume that all spatial gradients in the mean temperature equation scale as $\nabla = O\left(\overline{\ell}_T^{-1}\right)$ since these gradients act on mean thermal quantities; although the convective heat flux involves fluctuating quantities, we assume that the averaging operator filters the smallest $O(\mathrm{Ek}^{1/3})$ length scales. In what follows we assume that large-scale thermal diffusion must play a dominant role in the mean temperature equation to allow for a statistically stationary mean temperature field.

Balancing the convective heat flux and the large-scale thermal diffusion leads to

$$\nabla \cdot \left(\overline{u'T'}\right) \sim \frac{1}{\Pr} \nabla^2 \overline{T} \qquad \Rightarrow \qquad \overline{\ell}_T = O\left(\frac{1}{u'T'}\right), \tag{47}$$

where we have assumed $\Pr = O(1)$ and $\overline{T} = O(1)$ and, again, assume that all gradients acting on mean thermal quantities scale as $\overline{\ell}_T^{-1}$. Here $u^{'}$ is the magnitude of the fluctuating velocity vector. If we assume that the small scales must be geostrophically balanced

then the fluctuating velocity is expected to scale as (Julien *et al.* 1998; Calkins *et al.* 2015)

$$u' = O\left(\epsilon^{-1}\right). \tag{48}$$

Although the linear theory for convection in a spherical shell suggests that the three fluctuating velocity components do not scale asymptotically in the same way (Dormy *et al.* 2004), the above scaling represents the strongest (in terms of the exponent on ϵ) asymptotic scaling identified, and it is therefore the scaling that is most readily observable in the numerical data presented later. Using this scaling for the fluctuating velocity then leads to

$$\overline{\ell}_T = O\left(\frac{\epsilon}{T'}\right). \tag{49}$$

Another possible balance is between advection by the mean flow and thermal diffusion such that

$$\overline{u} \cdot \nabla \overline{T} \sim \frac{1}{\Pr} \nabla^2 \overline{T} \qquad \Rightarrow \qquad \overline{u}_s = O\left(\frac{1}{\overline{\ell}_T}\right).$$
 (50)

Finally, we note that combining the scalings for \overline{u}_s and $\overline{\ell}_T$ relates the fluctuating temperature to the meridional circulation

$$T' = O\left(\epsilon \overline{u}_s\right). \tag{51}$$

Whereas plane layer theory yields $T' = O(\epsilon)$ (Julien *et al.* 1998), the numerical data presented here does not support this scaling of the fluctuating temperature in the sphere; this point is discussed more later.

A possible scaling for $\overline{\ell}_T$ is the 'convective envelope' scale that varies like $\epsilon^{1/2} = \operatorname{Ek}^{1/6}$ (Jones *et al.* 2000); this length scale characterizes the radial width of the region that contains the smaller length scale $\epsilon = \operatorname{Ek}^{1/3}$ within which the thermal Rossby waves oscillate. We find *a posteriori* that this scale is consistent with the numerical data. Thus, the following asymptotic estimates are obtained

$$\nabla^2 \overline{T} = O\left(\epsilon^{-1}\right),\tag{52}$$

$$\overline{\boldsymbol{u}} \cdot \nabla \overline{T} = O\left(\overline{\boldsymbol{u}}_s \epsilon^{-1/2}\right). \tag{53}$$

Utilizing the balance between advection by the mean and thermal diffusion we therefore have

$$\overline{u}_s = O\left(\epsilon^{-1/2}\right),\tag{54}$$

and, from balancing the convective heat flux and thermal diffusion terms, we have the following scaling for the convective heat flux

$$\overline{u'_{r}T'} = O\left(\epsilon^{-1/2}\right). \tag{55}$$

Then, using the scaling $u'_r = O(\epsilon^{-1})$,

$$T' = O\left(\epsilon^{1/2}\right). \tag{56}$$

With an estimate for the scaling of \overline{u}_s , the Lorentz-Coriolis balance in the zonal momentum equation now suggests

$$\left(\overline{\boldsymbol{J} \times \boldsymbol{B}}\right)_{\phi} = O\left(\frac{1}{\overline{\ell}_{T}}\right). \tag{57}$$

The zonal component of the mean Lorentz force contains only magnetic tension since the averaging removes magnetic pressure gradients. The magnetic tension term can be split further into two terms, the mean—mean and eddy–eddy contributions. Since the derivatives appearing in those terms act on mean magnetic quantities, we assume that they scale as $\nabla = O\left(\overline{\ell}_B^{-1}\right)$. The two mean Lorentz force terms can then be written as

$$\left(\overline{B} \cdot \nabla \overline{B}\right)_{\phi} = O\left(\frac{\overline{B}^2}{\overline{\ell}_B}\right),\tag{58}$$

$$\left(\overline{\mathbf{B}' \cdot \nabla \mathbf{B}'}\right)_{\phi} = O\left(\frac{B'^2}{\overline{\ell}_B}\right). \tag{59}$$

Combining these with the scaling relation for the full mean zonal Lorentz force provides

$$\overline{B} = B' = O\left(\frac{\overline{\ell}_B^{1/2}}{\overline{\ell}_T^{1/2}}\right). \tag{60}$$

In the next section we attempt to constrain the possible scalings with ϵ using data from numerical simulations. However, if we assume that $\overline{\ell}_B$ and $\overline{\ell}_T$ both have the same scaling behaviour, then we find

$$\overline{B} = B' = O(1). \tag{61}$$

We note that application of the chain rule relating derivatives in the spherical coordinate system used here to derivatives in a cylindrical coordinate system requires that any length scale present in radius r and colatitude θ is also present in the axial (z) direction. For example, the curl of the thermal wind force balance (29) yields the well known relationship between the axial derivative of the zonal flow and the colatitudinal derivative of the mean temperature,

$$\frac{2}{\operatorname{Ek}} \frac{\partial \overline{u}_{\phi}}{\partial z} \approx \frac{Ra}{Pr} \frac{1}{r_o} \frac{\partial \overline{T}}{\partial \theta}.$$
 (62)

Assuming that the z-derivative on the left-hand side scales as $\overline{\ell}_T^{-1}$, the above relationship then reduces to relationship (40).

4 COMPARISON WITH NUMERICAL SIMULATIONS

In this section, we compare the arguments and scalings presented in the previous section with data from numerical dynamo models. Three criteria are used to assess whether a given quantity computed from the numerical simulations possesses asymptotic scaling behaviour: (1) the raw (unscaled) data must show evidence that the magnitude of the quantity systematically changes with the Ekman number; (2) the asymptotically rescaled data should be order unity in magnitude and (3) the asymptotic scaling must be consistent with the dominant balances observed in the numerical simulations.

The numerical simulation parameters are summarized in Table 1. Four different values of the Ekman number were used, $Ek=(10^{-4}, 3\times 10^{-5}, 10^{-5}, 3\times 10^{-6})$ and the Rayleigh number was varied for each Ekman number; the critical Rayleigh number for each Ekman number is $Ra_{crit}\approx (7.0\times 10^5, 2.8\times 10^6, 1.1\times 10^7, 4.6\times 10^7)$ (Christensen & Aubert 2006). Both the thermal and magnetic Prandtl numbers are fixed at Pr=1 and Pm=2, respectively. With the exception of the three largest Rayleigh number cases with $Ek=10^{-4}$ which exhibited multipolar dynamos, all cases were characterized by a dipole dominated magnetic field morphology; the larger the Rayleigh number, the less confidence we have that the small Rossby and small Ekman number theory will apply. We begin with a discussion of the mean temperature equation, followed by an analysis of the terms appearing in the mean momentum equation.

4.1 Mean temperature equation

Fig. 1 shows the rms value of all terms in the mean temperature eq. (46) as a function of Ekman number for cases in which $Ra = 15 Ra_{crit}$. The rms values were computed within the bulk of the volume, excluding the Ekman layers adjacent to the inner and outer boundaries, and subsequently averaged in time. It was found

Table 1. Details of the numerical simulations. The number of Chebyshev polynomials is denoted by n_r and $\ell_{\rm max}$ is the maximum spherical harmonic degree. The non-dimensional parameters are the Ekman number Ek, the magnetic Reynolds number Rm and the Rossby number Ro. For all simulations, the thermal Prandtl number and the magnetic Prandtl number are fixed at Pr=1 and Pm=2, respectively.

Ek	Ra	n_r	ℓ_{max}	Rm	Ro
10^{-4}	4.20×10^{6}	64	127	106.068	5.303×10^{-3}
10^{-4}	7.00×10^{6}	64	127	152.699	7.635×10^{-3}
10^{-4}	1.05×10^{7}	64	127	228.753	1.144×10^{-2}
10^{-4}	1.40×10^{7}	72	159	302.902	1.515×10^{-2}
10^{-4}	2.10×10^{7}	92	199	536.589	2.683×10^{-2}
10^{-4}	2.80×10^{7}	96	215	630.677	3.153×10^{-2}
10^{-4}	3.50×10^{7}	128	255	676.616	3.383×10^{-2}
3×10^{-5}	1.42×10^{7}	84	239	113.681	1.705×10^{-3}
3×10^{-5}	2.83×10^{7}	92	239	191.783	2.877×10^{-3}
3×10^{-5}	4.25×10^{7}	92	239	313.915	4.709×10^{-3}
3×10^{-5}	5.67×10^{7}	92	239	422.756	6.341×10^{-3}
3×10^{-5}	7.08×10^{7}	128	255	474.392	7.116×10^{-3}
3×10^{-5}	9.92×10^{7}	128	323	672.669	1.009×10^{-2}
3×10^{-5}	1.27×10^{8}	128	323	832.567	1.249×10^{-2}
3×10^{-5}	1.56×10^{8}	128	359	997.755	1.497×10^{-2}
10^{-5}	7.00×10^{7}	96	255	187.228	9.361×10^{-4}
10^{-5}	8.00×10^{7}	96	255	204.217	1.021×10^{-3}
10^{-5}	1.00×10^{8}	96	287	240.137	1.201×10^{-3}
10^{-5}	1.20×10^{8}	96	287	257.756	1.289×10^{-3}
10^{-5}	1.50×10^{8}	96	287	349.233	1.746×10^{-3}
10^{-5}	2.00×10^{8}	128	359	460.731	2.304×10^{-3}
3×10^{-6}	2.30×10^{8}	140	359	210.503	3.158×10^{-4}
3×10^{-6}	3.21×10^{8}	140	359	288.910	4.334×10^{-4}
3×10^{-6}	4.59×10^{8}	140	383	314.152	4.712×10^{-4}
3×10^{-6}	6.89×10^{8}	144	399	498.131	7.472×10^{-4}

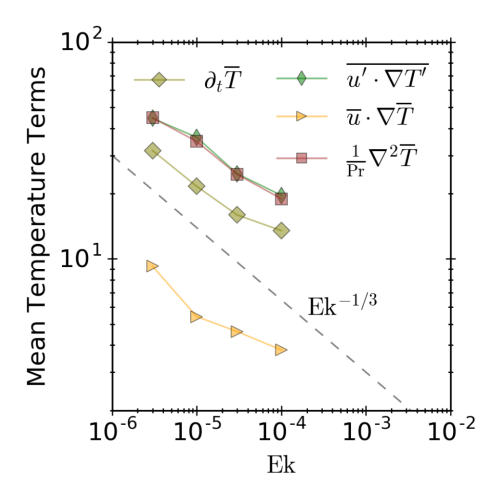


Figure 1. Scaling behaviour of all terms in the mean temperature equation. The rms value of each term is shown as a function of Ekman number with a fixed supercriticality $Ra\approx 15Ra_{crit}.$ The slope of $Ek^{-1/3}$ is shown for reference.

that including the Ekman layers had no significant difference in the computed values for the mean temperature equation. Here we exclude the Ekman layers to be consistent with the computation of the forces in the mean momentum equation. For reference, the dashed line shows a slope of $\epsilon^{-1} = \mathrm{Ek}^{-1/3}$. One obvious trend is that all terms in the equation increase in magnitude as the Ekman number is reduced for a fixed supercriticality. We also see that the convective heat flux is balanced with large-scale thermal diffusion. The time derivative is smaller than both the convective heat flux and thermal

diffusion by a factor of \approx 2/3. Finally, advection of heat by the mean flow is notably weaker than all of the other terms, and is a factor of \approx 1/5 smaller than either the convective flux or thermal diffusion over the investigated range of Ekman numbers.

It is clear that the advection of the mean temperature by the mean flow is small in comparison to the convective flux and thermal diffusion. However, the advection due to the mean flow increases in magnitude with decreasing Ekman number. This behaviour suggests that advection by the mean does have an Ekman number dependence, in agreement with the scaling analysis. Thus, this dependence might still be used to constrain the asymptotic size of the meridional circulation.

Whereas the time derivative of the mean temperature is smaller than both the convective heat flux and thermal diffusion, but it appears to scale with the Ekman number in a similar way. Balancing the time derivative with either of these two terms provides an estimate for the mean thermal evolution timescale

$$\partial_t \overline{T} = O\left(\tau^{-1}\right) \sim \nabla^2 \overline{T} = O\left(\epsilon^{-1}\right).$$
 (63)

This indicates that the mean thermal evolution timescale is, $\tau = O(\epsilon)$.

The Rayleigh number dependence of the terms in the mean heat equation is shown in Fig. 2 for each value of the Ekman number. In general, the scaling behaviour for each term in the equation is similar, both for fixed and varying Ekman number, showing an increase with the Rayleigh number. The balance between thermal diffusion and the divergence of the convective heat flux is robust so long as the Rossby number remains small. There is a loss of balance in the mean heat equation for the Ek = 10^{-4} cases in which $\widetilde{Ra} > 80$ and the Ek = 3×10^{-5} cases in which $\widetilde{Ra} > 60$. We also find that heat transport by the meridional circulation is of comparable relative size over the range of investigated Rayleigh numbers.

Fig. 3(a) shows the mean temperature length scale, calculated according to

$$\overline{\ell}_T = \left(\frac{\left\langle \overline{T}^2 \right\rangle}{\left\langle \left| \nabla^2 \overline{T} \right|^2 \right\rangle} \right)^{1/4},\tag{64}$$

where the angled brackets indicate a volume and time average. The Laplacian is used to calculate the length scale since it will naturally magnify small length scales, and therefore provide an estimate for any Ekman number dependent length scale. There is evidence that $\bar{\ell}_T$ decreases with Ek. If the data are rescaled by the inverse convective envelope scale, $\epsilon^{-1/2} = \text{Ek}^{-1/6}$, there is a collapse of the data, as shown in Fig. 3(b), indicating the following scaling for the mean temperature length scale

$$\overline{\ell}_T = O\left(\epsilon^{1/2}\right). \tag{65}$$

We recall that this scaling should hold for a fixed value of the Rayleigh number, or reduced Rayleigh number, in the sense that we still expect a Rayleigh number dependence of the mean temperature length scale. In addition to collapsing the data, the rescaling shown in Fig. 3(b) shows that the rescaled mean thermal diffusion length-scale is order unity, that is $\epsilon^{-1/2} \overline{\ell}_T = O(1)$. Furthermore, the data shows a relatively weak dependence on the Rayleigh number and perhaps a saturation at large enough values. However, we note that the large Rayleigh number cases for Ek = 10^{-4} and Ek = 3×10^{-5} are characterized by relatively large Rossby numbers (Table 1).

Fig. 4(a) shows the meridional circulation as a function of reduced Rayleigh number for all cases. There is some evidence of a

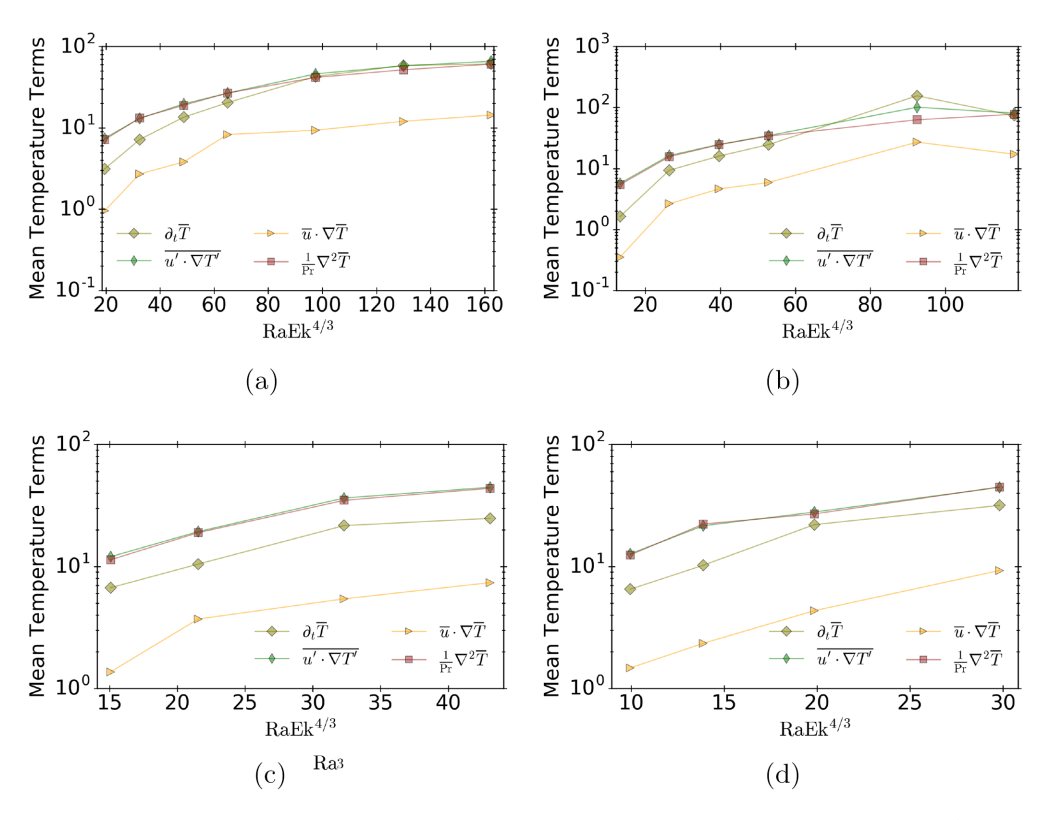


Figure 2. Scaling behaviour of all terms in the mean temperature equation as a function of reduced Rayleigh number, $RaEk^{4/3}$, for four different Ekman numbers: (a) $Ek = 10^{-4}$; (b) $Ek = 3 \times 10^{-5}$; (c) $Ek = 10^{-5}$ and (d) $Ek = 3 \times 10^{-6}$.

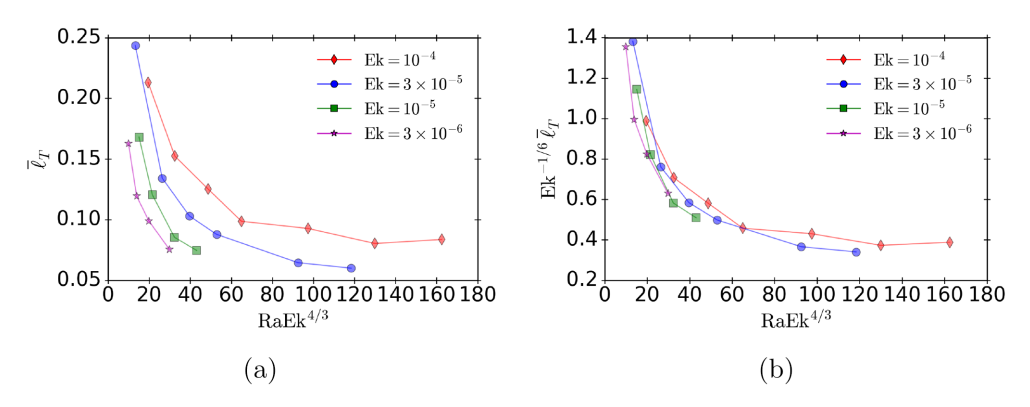


Figure 3. Scaling of the mean temperature length scale, $\overline{\ell}_T$, as a function of reduced Rayleigh number: (a) unscaled length scale and (b) length scale scaled with $\mathrm{Ek}^{-1/6}$.

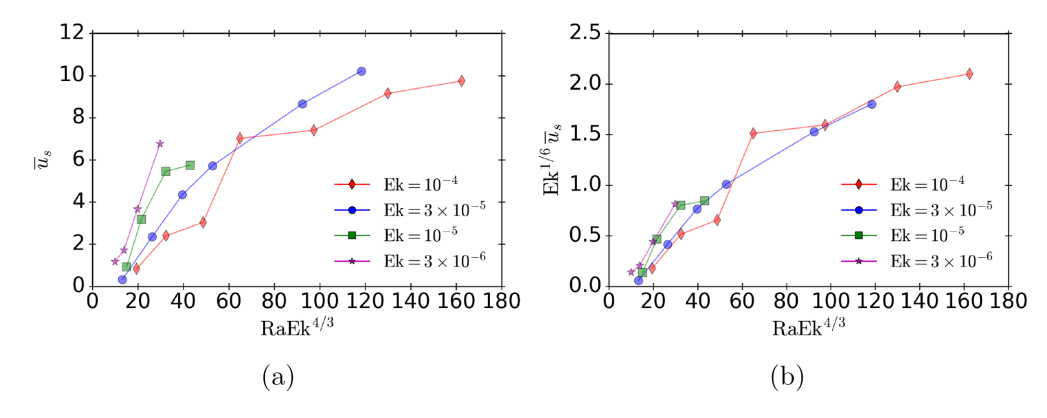


Figure 4. Scaling behaviour of the cylindrical radial component of the mean velocity (i.e. meridional circulation) as a function of reduced Rayleigh number: (a) rms meridional circulation and (b) rescaled meridional circulation.

dependence on Ek for some parameter values, showing larger values for smaller Ekman numbers. As shown in Fig. 4(b), scaling the meridional circulation by $\mathrm{Ek^{1/6}} = \epsilon^{1/2}$ provides some collapse of the data which may suggest

$$\overline{u}_s = O\left(\epsilon^{-1/2}\right),\tag{66}$$

in agreement with the estimate from the previous section. The physical origin of this scaling is unclear, though it may be tied to Ekman pumping which is known to become stronger in rotating convection with decreasing Ekman number and increasing Rayleigh number (Julien *et al.* 2016).

Fig. 5 shows various quantities relevant to the convective heat flux. The raw data for the fluctuating velocity is shown in Fig. 5(a) and shows a general trend of larger magnitudes with decreasing Ekman number and a steeper scaling with increasing (reduced) Rayleigh number; the rescaled fluctuating velocity in Fig. 5(b) shows that the previously suggested $Ek^{-1/3}$ scaling provides a collapse of the data. The convective heat flux shown in Fig. 5(c) illustrates similar scaling behaviour to both the fluctuating velocity and the meridional circulation, and the rescaled data in Fig. 5(d) shows collapse with a Ek1/6 scaling. Though not shown, this scaling for the convective heat flux is consistent with an equivalent scaling for the Nusselt number; this effect may be related to Ekman pumping—we refer the reader to Julie et al. (2016) and references cited therein. The rms of the fluctuating temperature shown in Fig. 5(e) does not show an obvious trend with Ekman number, such as the scaling analysis that led to eq. (56) would suggest. The lack of an obvious dependence of T on Ek is in disagreement with the scaling arguments presented previously. Radial profiles of the rms temperature perturbation are shown in Fig. 5(f) for a fixed supercriticality of Ra = 15 Ra_{crit} and the four different Ekman numbers considered here. These profiles show that the rms values of the temperature perturbation are not dependent upon how the rms is computed; for instance, whether Ekman layers are included or not. The reason for this lack of Ekman number dependence is not currently known. We have checked that our computed values of T' are consistent with previous calculations for the fluctuating buoyancy force (e.g. Yadav et al. 2016). An ongoing investigation of the fluctuating dynamics may yield insight into this behaviour.

4.2 Mean momentum equation

4.2.1 Pointwise analysis

Force balances, if present, are satisfied pointwise because the partial differential equations that govern such balances are satisfied locally in space (and time). Because our definition of 'large-scale' corresponds to axisymmetric quantities, this implies that balances on the large-scale are satisfied at all points (excluding boundary layers) in the meridional plane. Distinct balances can be present in different regions of the flow domain; for instance, within the Ekman layers near the inner and outer boundaries we expect different balances in comparison to the bulk. Schaeffer et al. (2017) have examined balances in the vorticity equation in five distinct regions. Other work has used global rms values of the forces that both include (Soderlund et al. 2012) and exclude the Ekman layers (Yadav et al. 2016), and Aubert et al. (2017) used a spectral decomposition of the forces. All results presented here do not include the Ekman layer when computing the global rms value. Here we extend these previous analyses to the mean dynamics, and to show how these large-scale balances are directionally distinct, and that such balances are separated by an asymptotically small parameter and therefore represent perturbative dynamics in the sense that a sequence of force balances is present, with each sequence separated by an asymptotically small parameter. The numerical data is used to help constrain the asymptotic ordering of the perturbative dynamics.

Fig. 6 shows the numerically computed forces for the particular case of Ek = 10^{-5} and Ra = 10 Ra_{crit} . All other small Rossby number cases show qualitatively similar behaviour. The figure shows the mean forces extracted at a particular point in space and plotted as a function of time. The spatial location is chosen to be $r \approx 0.74 r_o$ and a latitude of $\approx 40^{\circ}$, far-removed from the Ekman layer and the tangent cylinder region. Analyses at other locations show similar behaviour to the chosen data, provided such locations are outside of the Ekman layers. The radial and zonal components are shown in the left column and the right-hand column, respectively. The rows indicate the various orders of observed balances, with the primary force balance shown in the top row. Each subsequent higher order balance is shown with the sum of the terms appearing in the preceding lower order balance. The sequence of force balances in the radial direction is the following: (1) a leading order thermal wind balance between the (mean) Coriolis, pressure gradient, and buoyancy forces; (2) a secondary balance between the sum of the thermal wind terms and the mean Lorentz force and (3) a tertiary 'balance' where all forces become relevant. This latter balance is not a true balance since inertia becomes important at this order and the momentum equation is therefore prognostic, as opposed to the diagnostic balances that occur at lower order. We observe that the magnitude of the forces appearing in a given balance decreases by approximately one order of magnitude in each higher order balance; this difference is roughly consistent with an order $e^{1/2} = \text{Ek}^{1/6}$ perturbation parameter.

Though not shown, the colatitudinal component of the mean momentum equation shows similar behaviour to the radial component with forces of comparable magnitude and the same sequence of balances is observed.

The right column in Fig. 6 shows the pointwise computed forces in the zonal direction. Here we observe that the mean Coriolis force and the mean Lorentz force are in balance at leading order, as shown in Fig. 6(b) and expressed by eq. (30). All forces, including the viscous force, become important at the next order in the zonal direction, as shown in Fig. 6(d). Thus, based on the observed balances, the zonal dynamics are determined at second order. Like the sequence of force balances observed in the radial direction, we find that the two balances in the zonal direction differ by approximately one order of magnitude. Furthermore, we note that the leading order terms in the zonal direction are approximately one order of magnitude smaller than the leading order thermal wind balance in the meridional plane. As discussed previously, this directional difference in the size of the leading order balances provides an argument for characterizing the leading order balance in these spherical dynamos as a semi-MS balance since the Lorentz force enters only the zonal direction at leading order.

4.2.2 Global rms analysis

The point-wise analysis is useful for showing which forces balance, their time dependence, and at what asymptotic order they balance. However, to show how each force scales with ϵ , it is helpful to consider global rms values of the forces, as has been done previously for determining the Rayleigh number dependence of the fluctuating

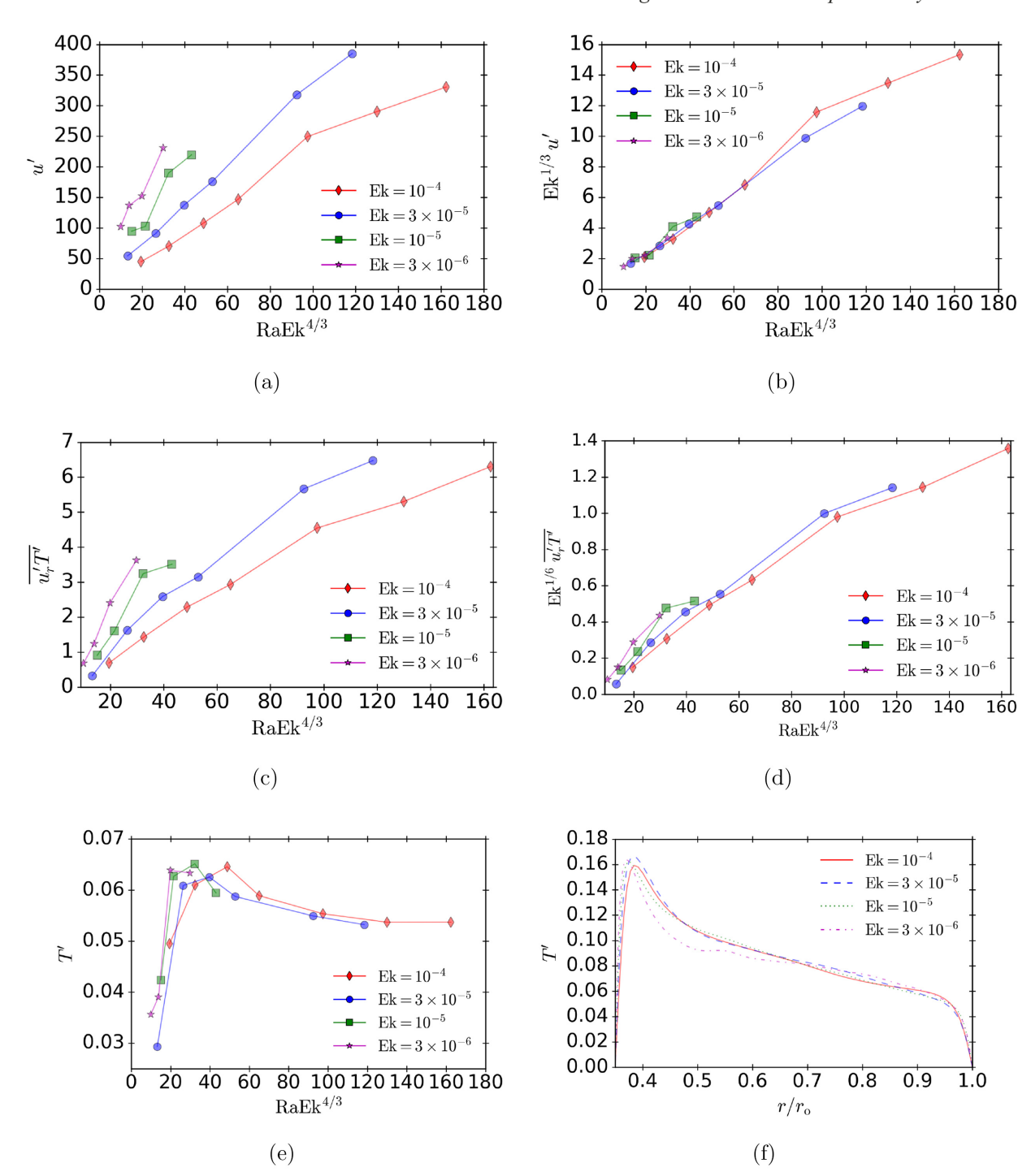


Figure 5. Scaling behaviour of (a, b) the fluctuating velocity; (c, d) the convective heat flux and (e, f) the fluctuating temperature. rms values of the various quantities and associated rescaled quantities are shown in (a)–(e); panel (f) shows radial profiles of the rms fluctuating temperature for all Ekman numbers with $Ra = 15 Ra_{crit}$.

forces (Soderlund *et al.* 2012; Yadav *et al.* 2016). We examine the mean balance both for fixed and varying supercriticality.

Fig. 7 shows the rms of the mean forces as a function of Ekman number for all cases with $Ra=10\,Ra_{crit}$. The cross symbols indicate the sum of the terms appearing in the primary semi-MS balance, and the plus symbols indicate the secondary force balance (for the radial direction). Asymptotic scaling slopes are shown for reference only; because the cases at different Ekman numbers are characterized by different Reynolds numbers we do not expect the data shown

to follow these scaling relations precisely. The radial forces are shown in Fig. 7(a); the primary thermal wind balance between the Coriolis, pressure gradient and buoyancy forces is evident, and the Lorentz force is consistently smaller than this primary balance by approximately an order of magnitude for all Ekman numbers. However, there is a slight trend showing that the relative size of the Lorentz force increases with decreasing Ekman number. As shown by the pointwise analysis, the magnitude of the sum of the thermal wind balance terms is very close to the magnitude of the

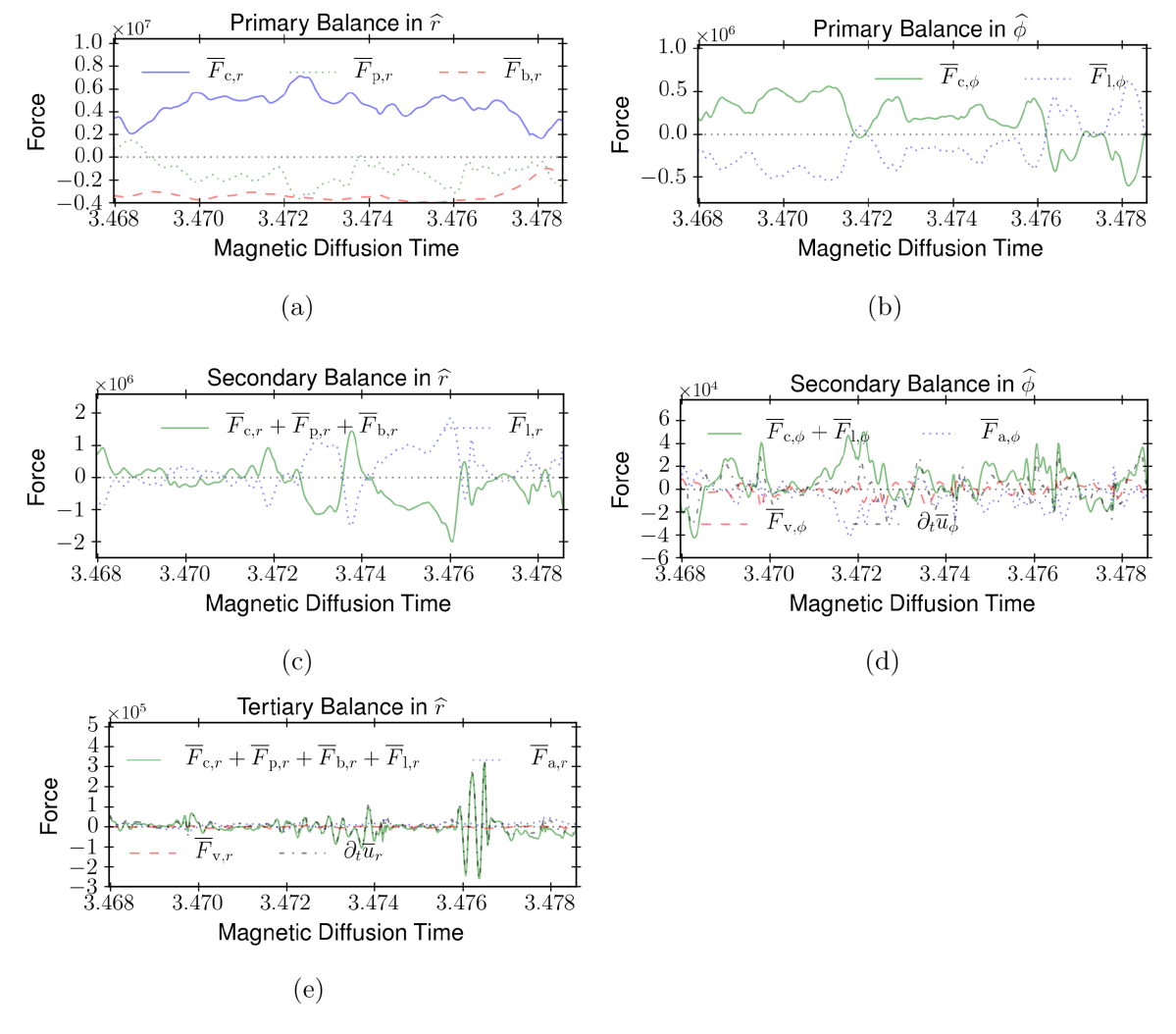


Figure 6. Pointwise measurements of forces (as a function of time) in the mean momentum equation at the point $(r, \theta) \approx (0.74 \, r_o, 40^\circ)$. The parameters are $Ek = 10^{-5}$, $Ra = 10 \, Ra_{crit}$. The left-hand column shows the radial direction and the right column shows the zonal direction. The top row shows the primary force balance and higher order balances are shown in the subsequent rows. The dotted black line indicates zero.

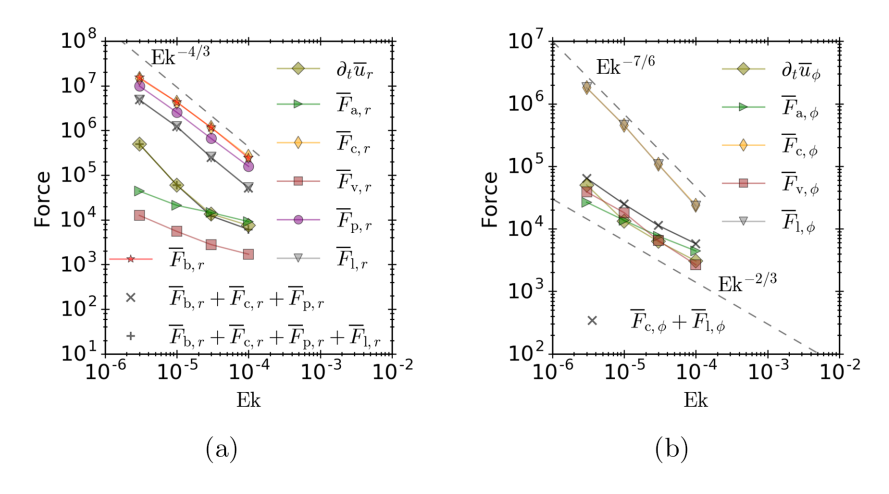


Figure 7. Global rms values of the mean forces as a function of the Ekman number: (a) radial components; (b) zonal components. In all cases the supercriticality is fixed at $Ra = 10 Ra_{crit}$. The rms of the sum of the primary force balance is marked with the 'x' symbols and the rms of the sum of the secondary force balance is shown by the '+' symbols.

Lorentz force, again suggesting that distinct perturbative balances are present in the large scale dynamics. Inertia, advection, and the viscous force are all small relative to the leading order thermal wind balance. Furthermore, these same three forces show a significantly weaker scaling behaviour with varying Ekman number, which is also evidence for perturbative dynamics. The plus symbols, showing the sum of the Coriolis, pressure gradient, buoyancy and Lorentz forces, are approximately the same magnitude as these three smallest forces.

Fig. 7(b) shows the zonal components of the mean forces for Ra = 10 Ra_{crit}. The primary Lorentz–Coriolis balance is evident, as is the steeper scaling behaviour with Ekman number in comparison to inertia, advection, and the viscous force. With the $\overline{u}_s = O(\epsilon^{-1/2})$ scaling, the zonal components of the mean Coriolis force and the mean Lorentz force should scale as $\epsilon^{-7/2} = \text{Ek}^{-7/6}$; this scaling is shown in the Figure. The sum of the Lorentz and Coriolis forces is approximately equal in magnitude to these three smaller forces. We note that the prognostic dynamics (e.g. torsional oscillations) enter at this higher order. We also see that all three of these higher order forces scale similarly with the Ekman number, and that they are all of comparable magnitude, indicating that they are all important in the dynamics at this order. While the viscous force is the smallest in magnitude, it nevertheless scales approximately in the same way as inertia and advection.

To better understand the Rayleigh number dependence of the forces, Figs 8 and 9 show the radial and zonal components of the mean forces, respectively, for each of the Ekman numbers considered here, as a function of the reduced Rayleigh number. All Ekman numbers show evidence of a semi-MS balance provided the Rayleigh number is not too large. The data shows that for the three highest Rayleigh number simulations for $Ek = 10^{-4}$ and the two highest Rayleigh number simulations for $Ek = 3 \times 10^{-5}$, there is a loss of balance since both advection and inertia become comparable in magnitude to the zonal component of the Coriolis force. This loss of balance is particularly notable for the $Ek = 10^{-4}$ simulations with Ra > 80. As previously mentioned, the colatitudinal component of the forces shows similar behaviour to the radial component and it is therefore omitted for brevity.

The rms mean buoyancy force is shown in Fig. 10, for both the raw (unscaled) and rescaled data. A systematic increase in the magnitude of the mean buoyancy force is noted in Fig. 10(a), whereas the rescaled data in Fig. 10(b) shows that all of the cases collapse and become order unity. This data provides strong support for our initial assumptions that $\overline{T} = O(1)$ and $Ra = O(Ek^{-4/3})$.

We now examine the Ekman number dependence of the various dependent variables and length scales that were analysed and introduced using the method of dominant balance in Section 3. We found that the thermal wind balance in the meridional plane requires that the mean zonal velocity scales $\overline{u}_{\phi} \sim \text{Ek}^{-1/3}$, per eq. (37). Fig. 11 shows the scaling behaviour of the zonal component of the mean velocity, with the raw and rescaled data shown in Figs 11(a) and (b), respectively. We find that the scaling of $\overline{u}_{\phi} \sim \text{Ek}^{-1/3}$ leads to a collapse of the data, suggesting that the thermal wind balance is maintained in the mean dynamics over the parameter space investigated. Note that the sudden change, or 'kink', in the zonal flow data for $E=3\times10^{-6}$ observable in (a) is the result of a change in the structure of the zonal flow for this particular case; the cause of this behaviour is currently unknown.

The scaling relations for the mean and fluctuating magnetic field obtained in the previous section were written as

$$\overline{B} = B' = O\left(\frac{\overline{\ell}_B^{1/2}}{\overline{\ell}_r^{1/2}}\right). \tag{67}$$

As previously mentioned, the data suggests that an estimate for the scaling of the mean temperature length scale is $\overline{\ell}_T = O\left(\epsilon^{1/2}\right)$. Computing the mean magnetic field length scale in the same way as for the mean temperature length scale (i.e. using the Laplacian) yields the data shown in Fig. 12(a). Fig. 12(b) shows the data rescaled by Ek^{-1/6} where a collapse for the lower Rossby number cases is observed; the higher Rossby number cases for Ek = 10^{-4} deviate most significantly from this Ekman number scaling.

The rms of both the mean and the fluctuating magnetic field are plotted in Fig. 13. We find that the magnitudes of both quantities, in our non-dimensional units, are order unity. For a given Ekman number and Rayleigh number, the fluctuating magnetic field is larger in magnitude than the mean magnetic field. The fluctuating magnetic field shows a systematic trend of increasing magnitude with decreasing Ekman number. However, despite this trend, the values remain order unity within the parameter space investigated. Although it is possible to collapse the data for the fluctuating magnetic field, we found that this yielded rescaled values that were o(1). In addition, a true asymptotic dependence in the fluctuating magnetic field would violate the observed semi-MS balance. The observed trend in the rms of the fluctuating magnetic field may be due to the fact that smaller Ekman number dynamos are intrinsically more efficient at producing dynamo action, though not in an asymptotic sense. As previously mentioned with regard to the fluctuating temperature behaviour, further investigations into the fluctuating force balances may shed light on the observed behaviour of the fluctuating magnetic field.

A summary of the scaling relationships that are consistent with the numerical data are shown in Table 2. The scaling relationships discussed in the previous section are consistent with the numerically observed scaling behaviour for several quantities. In particular, the scaling arguments appear to capture the scaling behaviour of the mean meridional circulation, the mean zonal velocity and the fluctuating velocity. The most notable discrepancy between the asymptotic predictions and the observed behaviour is for the fluctuating temperature, which shows no clear Ekman number dependence. In addition, an Ekman number dependence is observed in the scaling behaviour of the fluctuating magnetic field, though the observed magnitudes remain order one across the Ekman numbers investigated here. These discrepancies may arise from the assumptions that were used in the simplified balance analysis. In particular, a more detailed analysis that does not rely on the assumption of a single Ekman number dependent length scale may prove to be more accurate in identification of asymptotic behaviour.

5 COMMENTS ON TAYLOR'S CONSTRAINT AND TORSIONAL OSCILLATIONS

As first shown by Taylor (1963), if we integrate the zonal component of the large-scale force balance in the direction along the rotation axis we obtain Taylor's constraint

$$\int_{-h}^{h} \widehat{\boldsymbol{\phi}} \cdot (\overline{\boldsymbol{J} \times \boldsymbol{B}}) \, dz \approx 0. \tag{68}$$

Through conservation of mass, the Coriolis term vanishes when integrated over the height of the outer boundary $h \equiv \sqrt{r_o^2 - s^2}$ (measured from the equatorial plane) for some cylindrical radius $s \equiv r \sin \theta$

We note that satisfying Taylor's constraint does not require a leading order magnetostrophic balance since the constraint applies

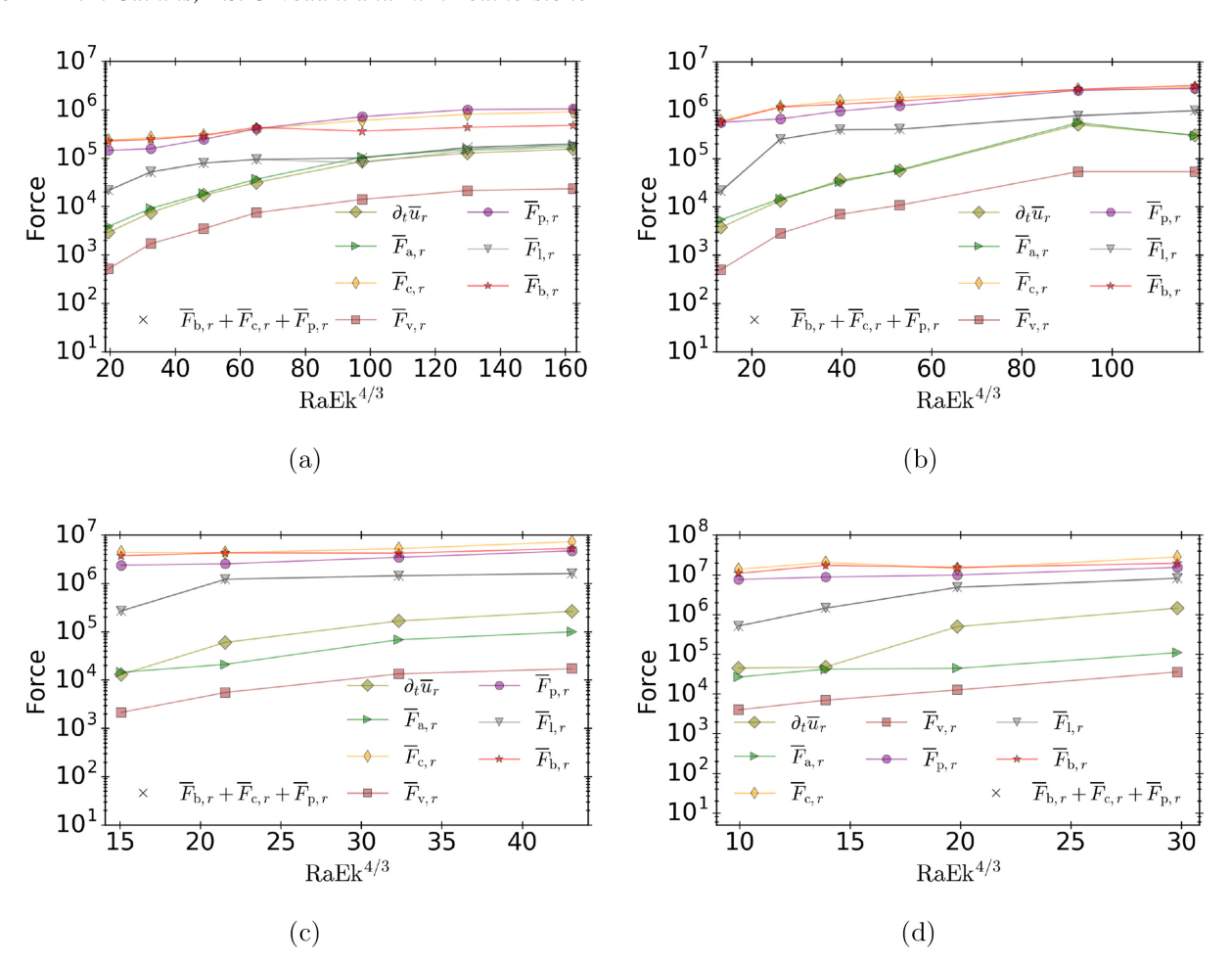


Figure 8. Scaling behaviour of the radial component of the mean forces as a function of reduced Rayleigh number for four different Ekman numbers: (a) Ek = 10^{-4} ; (b) Ek = 3×10^{-5} ; (c) Ek = 10^{-5} and (d) Ek = 3×10^{-6} .

only to the zonal component of the mean momentum equation. In this work, we provide arguments and numerical data that suggests the large-scale force balance in rapidly rotating convection-driven dynamos is more accurately termed semi-magnetostrophic since the Lorentz force is asymptotically smaller (at least for the parameter values considered here) than the largest terms in the mean momentum equation (e.g. the mean buoyancy force). Our analysis suggests, however, that this asymptotic difference is modest, since the leading order terms in the meridional and zonal components appear to be separated asymptotically only by $O(Ek^{1/6})$ if we compare the mean Lorentz force to the mean buoyancy force. This small difference may be one of the reasons that dynamo simulations do not show a strong satisfaction of Taylor's constraint (e.g. Schaeffer et al. 2017). Our analysis and numerical results suggest that the Reynolds stress term and the viscous term in the zonal component of the mean momentum equation are of size $O(Ek^{-5/6})$ and $O(Ek^{-2/3})$, respectively.

Taylor's constraint is often interpreted as implying that the large-scale dynamics of spherical dynamos are characterized by axially-invariant motions consisting of 'rigid' cylindrical annuli. There are two problems with this interpretation within the context of the present work. First, we recall that the large-scale meridional force balance is thermal wind, that is the mean buoyancy force enters at leading order. Because of this leading order thermal wind balance, the Taylor-Proudman theorem does not apply and we therefore expect zonal motions to exhibit leading order variations along the rotation axis (Aubert 2005). The analysis in Braginsky (1970) of

torsional oscillations relied on the absence of the buoyancy force: only if the buoyancy force is absent would we expect to see axial invariance in the dynamics at leading order (see e.g., Jault 2008). While many previous studies find evidence for axially-invariant torsional oscillations in numerical simulations driven by convection, this is likely due to a preference for equatorially symmetric motions. rather than a preference for axially invariant motions; the operation of axially-averaging would preferentially select this component of the flow. Secondly, the leading order Coriolis-Lorentz force balance in the zonal component of the mean momentum equation is satisfied in a pointwise fashion. This pointwise balance indicates that there is no net torque on any 'ring' of fluid (with the axis of the ring coincident with the rotation axis), suggesting that torsional oscillations are pointwise in the meridional plane. Taken together, these arguments suggest that the semi-MS force balance will yield large-scale wave motion that is not limited to axially invariant motion.

6 CONCLUSIONS

We have presented an analysis of the large-scale balances in convection-driven dynamos in a rotating spherical shell, both in the mean momentum equation and in the mean heat equation. The numerical data shows that, for a fixed supercritical Rayleigh number, all terms present in these two mean equations increase in magnitude as the Ekman number is decreased. It is the rate of this increase for each term in the equations that determines the dominant balances

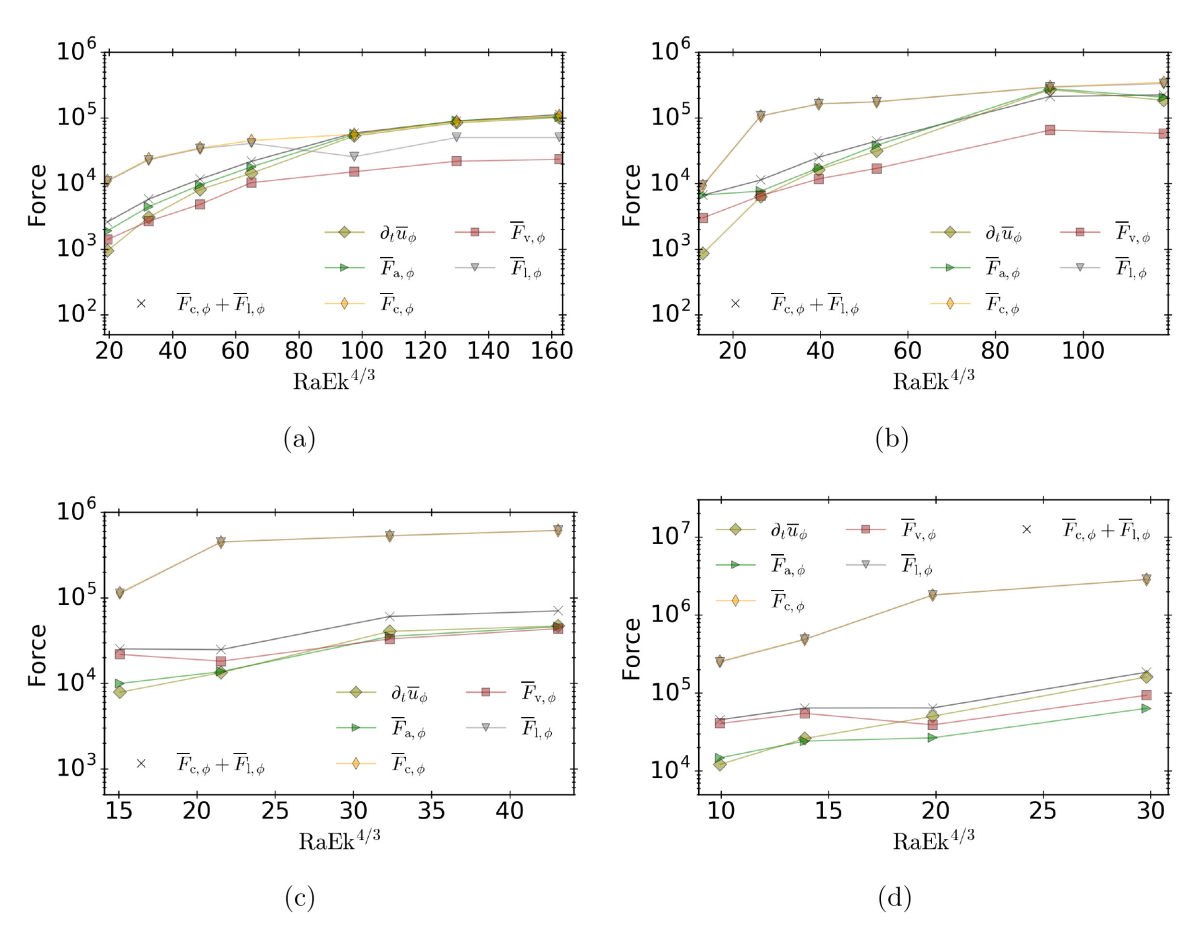


Figure 9. Scaling behaviour of the zonal component of the mean forces as a function of reduced Rayleigh number for four different Ekman numbers: (a) Ek = 10^{-4} ; (b) Ek = 3×10^{-5} ; (c) Ek = 10^{-5} and (d) Ek = 3×10^{-6} .

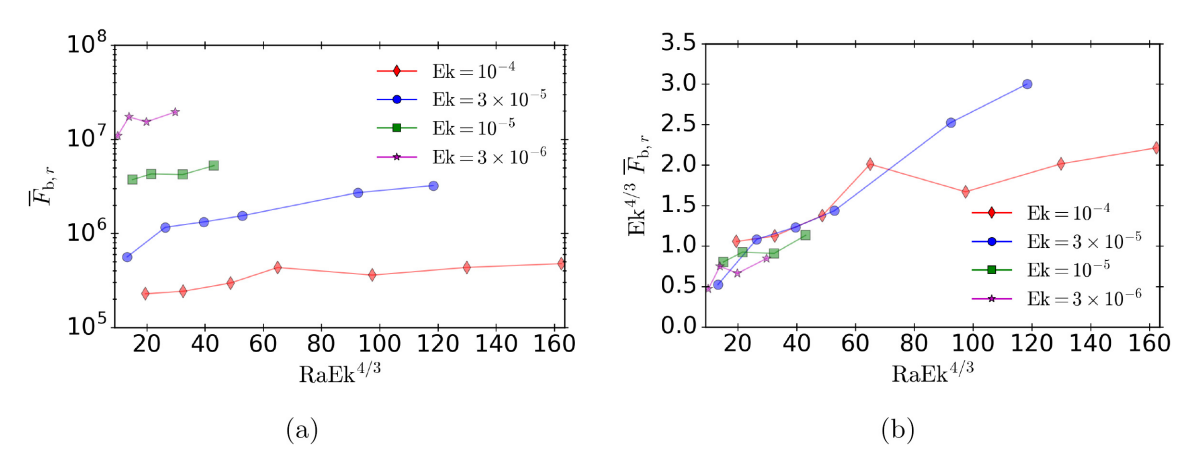


Figure 10. Scaling behaviour of the mean buoyancy force as a function of reduced Rayleigh number: (a) rms mean buoyancy force and (b) rms mean buoyancy force rescaled by Ek^{4/3}.

and the associated perturbative dynamics. Identifying these scalings is important for relating the results of numerical simulations to natural dynamos since computational restrictions limit the accessible range of parameter space in the former. Arguments, derived from the theory of rapidly rotating convection, were given that attempted to explain the physical origin of these rates, or asymptotic scalings, and a comparison was made with the output of numerical dynamo simulations.

With respect to the leading order force balances, the numerical simulations presented here are in agreement with previous studies that show a thermal wind balance in the meridional directions and a Coriolis–Lorentz balance in the zonal direction (Aubert 2005; Wicht & Christensen 2010; Sheyko *et al.* 2018). Our results show that these large-scale balances are robust across varying Ekman and Rayleigh numbers, provided the Rossby number remains small. The analysis shows that if the Rayleigh number scales as Ra =

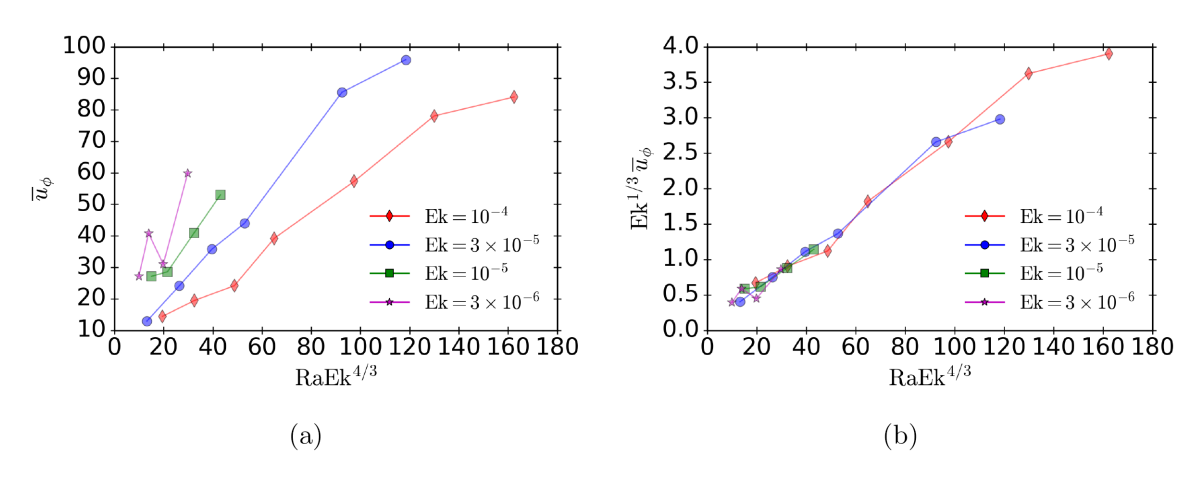


Figure 11. Scaling behaviour of the zonal flow speeds as a function of reduced Rayleigh number: (a) rms of the mean zonal velocity and (b) zonal flow speed rescaled by $Ek^{1/3}$.

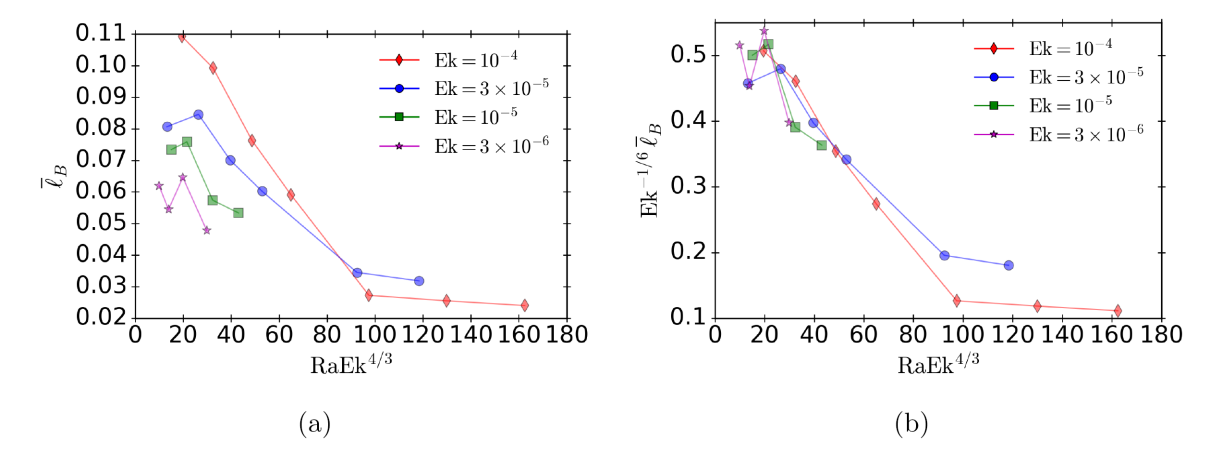


Figure 12. Length scale for the mean magnetic field as a function of reduced Rayleigh number: (a) raw data and (b) data rescaled by $Ek^{-1/6}$.

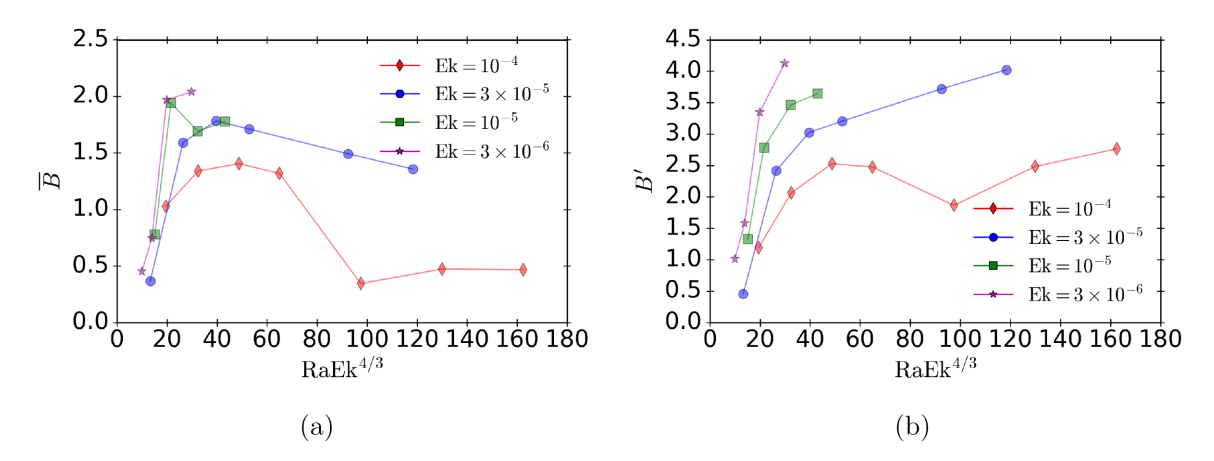


Figure 13. Scaling behaviour of (a) the mean and (b) the fluctuating magnetic field as a function of the reduced Rayleigh number.

 $O({\rm Ek}^{-4/3})$ (as it must in small Rossby number convection), the thermal wind balance requires that the zonal component of the mean velocity must scale as $\overline{u}_{\phi} = O\left({\rm Ek}^{-1/3}\right)$. We argue that one method for constraining the asymptotic size of the zonal components of the forces is to examine possible balances in the mean heat equation. The numerical results show that the mean heat equation is characterized by a balance between large-scale thermal diffusion and the divergence of the convective heat flux, indicating that both the mean

temperature and the convective heat flux vary on a $O(\mathrm{Ek}^{1/6})$ length scale, which is consistent with the convective envelope scale identified in linear theory (Jones *et al.* 2000). Whereas heat transport by the meridional circulation is weak relative to the dominant balance, it nevertheless shows an Ekman number dependence and indicates that the meridional circulation scales as $O(\mathrm{Ek}^{-1/6})$, and is therefore weaker than the corresponding scaling for the zonal flow. The scaling of the meridional circulation suggests that in order to have a

Table 2. Summary of suggested Ekman number (Ek) scalings for various quantities, with a reference					
to the figure where it first appeared. We list scalings that are, at a minimum, consistent with the					
numerical data.					

Quantity (symbol)	Scaling	Figure	Description
$\overline{\overline{T}}$	O(1)	-	mean temperature
$T^{'}$	O(1)	Fig. 5 (e)	fluctuating temperature
u'	$O(Ek^{-1/3})$	Figs 5(a,b)	fluctuating velocity
$\overline{u'_r T'}$	$O(Ek^{-1/6})$	Figs 5(c,d)	convective heat flux
\overline{u}_{ϕ}	$O(Ek^{-1/3})$	Figs 11(a,b)	mean zonal velocity
$\frac{\overline{u}_s}{\overline{B}}$	$O(Ek^{-1/6})$	Figs 4(a,b)	mean meridional circulation
	O(1)	Fig. 13(a)	mean magnetic field
$B^{'}$	O(1)	Fig. 13(b)	fluctuating magnetic field
$\overline{\ell}_T$	$O(Ek^{1/6})$	Figs 3(a,b)	length scale for mean temperature
$\overline{\ell}_B$	$O(\mathrm{Ek}^{1/6})$	Figs 12(a,b)	length scale for mean magnetic field

Coriolis-Lorentz force balance, the mean magnetic field (and the corresponding Maxwell stresses) should vary on a $O(Ek^{1/6})$ length scale, similar to the mean thermal quantities.

We observe a sequence of force balances in the mean momentum equation, indicating that the system is dynamically perturbative. The separation in magnitude between the various balances is consistent with small parameter of size $O(Ek^{1/6})$. However, given the limited range in Ekman numbers presented, we are aware that rigorously testing this scaling is currently not possible; however, the data is not inconsistent with this scaling. The zonal component of the mean momentum equation shows a robust leading order Coriolis–Lorentz force balance, with higher order dynamics that are influenced by both the viscous force and Reynolds stresses, as well as the 'reduced' Coriolis and Lorentz forces.

Not surprisingly, the multipolar dynamo cases for $\rm Ek=10^{-4}$ show evidence of a loss of balance, which is particularly evident in the zonal component of the mean momentum equation in which inertia and advection become as large as the Coriolis and Lorentz forces. In addition, for these same cases, there is a loss of balance in the mean temperature equation. These results are not inconsistent with the local Rossby number criteria for distinguishing dynamos with dipole-dominated magnetic fields and those with multipolar magnetic fields, which implicitly suggests a loss of rotational constraint (Christensen & Aubert 2006).

We do not observe a notable Ekman number dependence in the scaling of the fluctuating temperature. This lack of scaling is odd given that a geostrophic force balance holds on the small scales (Soderlund et al. 2012; Yadav et al. 2016), which implies that T' = o(1) (Julien et al. 1998). In our non-dimensional units, the rms temperature perturbations reach maximum values of ≈ 0.06 , which would make the fluctuating buoyancy force weaker than the fluctuating Coriolis force, as required for geostrophic balance (in contrast to thermal wind balance in which the buoyancy force is the same order of magnitude as the Coriolis force). It may be that this small value, while not asymptotic, is what separates the relative sizes of these forces. An ongoing investigation of the fluctuating dynamics may yield insight into this perplexing behaviour of the fluctuating temperature.

The numerical simulations do not show evidence of a leading order, large-scale magnetostrophic balance. Rather, the mean Lorentz force in the meridional components always seems to be balanced by the residual of the Coriolis, pressure gradient and buoyancy forces. For these reasons, we suggest that such dynamos should be termed semi-magnetostrophic since the mean Lorentz force only enters the leading order of a single component of the mean momentum equation. Despite the lack of a magnetostrophic balance,

we argue that Taylor state (large-scale) dynamos are still achieved because Taylor's constraint applies only to the zonal component of the momentum equation. Assuming our results and analysis hold at lower Ekman number, this suggests that Taylor's constraint should be satisfied up to $O(Ek^{1/6})$ for our simulations, which is a relatively weak asymptotic dependence that is consistent with the findings of previous simulations in which Taylor's constraint is only satisfied to an accuracy of about one part in ten (Schaeffer *et al.* 2017).

Although we have attempted to shed light on the multiscale dynamics of planetary interiors with the use of an asymptotic interpretation of numerical simulation results, our approach comes with many limitations. Because of the relatively weak asymptotic dependence of the scalings [e.g. powers of $O(\mathrm{Ek}^{1/6})$], the limited range in Ekman numbers available implies these scalings cannot be rigorously tested at present. Extending the present results to lower Ekman numbers would allow for better constraints on the scalings, though such an effort is computationally demanding. Our definition of the mean (large-scale) dynamics focuses only on the azimuthally averaged flows. It seems plausible that non-axisymmetric 'large-scale' motions might also important.

It is often assumed that the interior dynamics of the Earth and other planets are independent of viscosity. Attempts are often made to derive scaling laws for various quantities that do not depend on viscosity (Davidson 2013; Yadav *et al.* 2013b, a; Schrinner *et al.* 2014; Davidson 2014; Gastine *et al.* 2014; Jermyn *et al.* 2020a, b). While such a view is certainly possible, an alternative view, and one that is supported by the present analysis, is that planetary interior dynamics depend on viscosity in an asymptotic manner, rather than being completely independent of viscosity. This latter view is well known for explaining the linear dynamics of rotating spherical convection, and our present analysis suggests it may also be used for understanding certain aspects of the non-linear dynamics. That the numerical simulations show well-defined perturbative dynamics supports this asymptotic view.

ACKNOWLEDGEMENTS

The authors are grateful for the helpful comments of two anonymous referees. This work was supported by the National Science Foundation (NSF) under award numbers EAR-1620649 (MAC), EAR-1945270 (MAC) and SPG-1743852 (MAC, RJO), and by the National Aeronautics and Space Administration (NASA) under awards 80NSSC17K0008 (NAF) and 80NSSC20K0193 (NAF). The code Rayleigh was developed through the NSF-funded Computational Infrastructure for Geodynamics and supported by NSF

award numbers NSF-0949446 and NSF-1550901. This work utilized the RMACC Summit supercomputer, which is supported by the National Science Foundation (awards ACI-1532235 and ACI-1532236), the University of Colorado Boulder, and Colorado State University. The Summit supercomputer is a joint effort of the University of Colorado Boulder and Colorado State University. This work used the Extreme Science and Engineering Discovery Environment (XSEDE) Stampede2 at the Texas Advanced Computing Center through allocation TG-PHY180013.

DATA AVAILABILITY

Any data reported within this work is available upon request to the authors.

REFERENCES

- Amit, H. & Olson, P., 2004. Helical core flow from geomagnetic secular variation, *Phys. Earth planet. Int.*, 147, 1–25.
- Amit, H., Leonhardt, R. & Wicht, J., 2010. Polarity reversals from paleomagnetic observations and numerical dynamo simulations, *Space Sci. Rev.*, 155(1), 293–335.
- Aubert, J., 2005. Steady zonal flows in spherical shell dynamos, J. Fluid Mech., 542, 53-67.
- Aubert, J., Gastine, T. & Fournier, A., 2017. Spherical convective dynamos in the rapidly rotating asymptotic regime, J. Fluid Mech., 813, 558–593.
- Aurnou, J. & King, E., 2017. The cross-over to magnetostrophic convection in planetary dynamo systems, *Proc. R. Soc.*, 473(2199),.
- Aurnou, J.M., Calkins, M.A., Cheng, J.S., Julien, K., King, E.M., Nieves, D., Soderlund, K.M. & Stellmach, S., 2015. Rotating convective turbulence in Earth and planetary cores, *Phys. Earth planet. Int.*, 246, 52–71.
- Braginsky, S., 1970. Torsional magnetohydrodynamics vibrations in the Earth's core and variations in day length, *Geomagn. Aeron.*, 10, 3–12.
- Braginsky, S.I., 1976. On the nearly axially-symmetrical model of the hydromagnetic dynamo of the earth, *Phys. Earth planet. Int.*, 11(3), 191–199.
- Busse, F.H., 1970. Thermal instabilities in rapidly rotating systems., J. Fluid Mech., 44, 441–460.
- Calkins, M.A., 2018. Quasi-geostrophic dynamo theory, *Phys. Earth planet. Int.*, 276, 182–189.
- Calkins, M.A., Julien, K. & Marti, P., 2013. Three-dimensional quasigeostrophic convection in the rotating cylindrical annulus with steeply sloping endwalls, J. Fluid Mech., 732, 214–244.
- Calkins, M.A., Julien, K., Tobias, S.M. & Aurnou, J.M., 2015. A multiscale dynamo model driven by quasi-geostrophic convection, *J. Fluid Mech.*, 780, 143–166.
- Chandrasekhar, S., 1961. Hydrodynamic and Hydromagnetic Stability, Dover
- Christensen, U. & Aubert, J., 2006. Scaling properties of convection-driven dynamos in rotating shells and applications to planetary magnetic fields, *Geophys. J. Int.*, 166, 97–114.
- Davidson, P., 2013. Scaling laws for planetary dynamos, *Geophys. J. Int.*, 195(1), 67–74.
- Davidson, P.A., 2014. The dynamics and scaling laws of planetary dynamos driven by inertial waves, *Geophys. J. Int.*, 198(3), 1832–1847.
- Dormy, E., Soward, A.M., Jones, C.A., Jault, D. & Cardin, P., 2004. The onset of thermal convection in rotating spherical shells, *J. Fluid Mech.*, 501, 43–70
- Dormy, E., Soward, A.M., Jones, C.A., Jault, D. & Cardin, P., 2004. The onset of thermal convection in rotating spherical shells, *J. Fluid Mech.*, **501**, 43–70.
- Featherstone, N.A. & Hindman, B.W., 2016. The spectral amplitude of stellar convection and its scaling in the high-Rayleigh-number regime, *Astrophys. J.*, 818, 32,.
- Gastine, T., Heimpel, M. & Wicht, J., 2014. Zonal flow scaling in rapidly-rotating compressible convection, *Phys. Earth planet. Inter.*, 232, 36–50.

- Gillet, N., Jault, D., Canet, E. & Fournier, A., 2010. Fast torsional waves and strong magnetic field within the Earth's core, *Nature*, 465(7294), 74–77
- Gillet, N., Jault, D. & Finlay, C.C., 2015. Planetary gyre, time-dependent eddies, torsional waves, and equatorial jets at the Earth's core surface, *J. geophys. Res.*, 120, 3991–4013.
- Grooms, I., Julien, K. & Fox-Kemper, B., 2011. On the interactions between planetary geostrophy and mesoscale eddies, *Dyn. Atmos. Oceans*, 51, 109–136.
- Guervilly, C., Cardin, P. & Schaeffer, N., 2019. Turbulent convective length scale in planetary cores, *Nature*, 570(7761), 368–371.
- Hardy, C.M., Livermore, P.W., Niesen, J., Luo, J. & Li, K., 2018. Determination of the instantaneous geostrophic flow within the three-dimensional magnetostrophic regime, *Proc. R. Soc. A*, 474(2218), 20180412.
- Hulot, G., Eymin, C., Langlais, B., Mandea, M. & Olsen, N., 2002. Small-scale structure of the geodynamo inferred from Oersted and Magsat satellite data, *Nature*, 416, 620–623.
- Jault, D., 2008. Axial invariance of rapidly varying diffusionless motions in the Earth's core interior, *Phys. Earth planet. Int.*, 166(1-2), 67–76.
- Jermyn, A.S., Chitre, S.M., Lesaffre, P. & Tout, C.A., 2020a. Convective differential rotation in stars and planets–I. Theory, Mon. Not. R. astr. Soc., 498(3), 3758–3781.
- Jermyn, A.S., Chitre, S.M., Lesaffre, P. & Tout, C.A., 2020b. Convective differential rotation in stars and planets–II. Observational and numerical tests, *Mon. Not. R. astr. Soc.*, 498(3), 3782–3806.
- Jones, C.A., Soward, A.M. & Mussa, A.I., 2000. The onset of thermal convection in a rapidly rotating sphere, J. Fluid Mech., 405(1), 157–179.
- Julien, K. & Knobloch, E., 2007. Reduced models for fluid flows with strong constraints, J. Math. Phys., 48, doi:10.1063/1.2741042.
- Julien, K., Knobloch, E. & Werne, J., 1998. A new class of equations for rotationally constrained flows, *Theoret. Comput. Fluid Dyn.*, 11, 251–261.
- Julien, K., Aurnou, J.M., Calkins, M.A., Knobloch, E., Marti, P., Stellmach, S. & Vasil, G.M., 2016. A nonlinear model for rotationally constrained convection with Ekman pumping, J. Fluid Mech., 798, 50–87.
- King, E.M., Soderlund, K.M., Christensen, U.R., Wicht, J. & Aurnou, J.M., 2010. Convective heat transfer in planetary dynamo models, *Geochem. Geophys. Geosyst.*, 11(6), doi:10.1029/2010GC003053.
- Li, K., Jackson, A. & Livermore, P.W., 2018. Taylor state dynamos found by optimal control: axisymmetric examples, J. Fluid Mech., 853, 647–697.
- Livermore, P.W., Bailey, L.M. & Hollerbach, R., 2016. A comparison of noslip, stress-free and inviscid models of rapidly rotating fluid in a spherical shell, *Sci. Rep.*, **6**, 22812, doi:10.1038/srep22812.
- Livermore, P.W., Hollerbach, R. & Finlay, C.C., 2017. An accelerating highlatitude jet in Earth's core, *Nature Geo.*, **10**, 62–68.
- Maffei, S., Krouss, M.J., Julien, K. & Calkins, M.A., 2021. On the inverse cascade and flow speed scaling behaviour in rapidly rotating Rayleigh— Bénard convection, *J. Fluid Mech.*, 913, doi:10.1017/jfm.2020.1058.
- Malkus, W. V.R. & Proctor, M. R.E., 1975. The macrodynamics of α-effect dynamos in rotating fluids, *J. Fluid Mech.*, **67**, 417–443.
- Matsui, H. et al., 2016. Performance benchmarks for a next generation numerical dynamo model, Geochem. Geophys. Geosyst., 17, 1586–1607.
- Phillips, N.A., 1963. Geostrophic motion, Rev. Geophys., 1(2), 123-176.
- Pozzo, M., Davies, C.J., Gubbins, D. & Alfé, D., 2013. Transport properties for liquid silicon-oxygen-iron mixtures at Earth's core conditions, *Phys. Rev. B*, 87, doi:10.1103/PhysRevB.87.014110.
- Roberts, P.H., 1968. On the thermal instability of a rotating-fluid sphere containing heat sources, *Phil. Trans. R. Soc. A*, **263**(1136), 93–117.
- Roberts, P.H. & Aurnou, J.M., 2012. On the theory of core-mantle coupling, *Geophys. Astrophys. Fluid Dyn.*, **106**(2), 157–230.
- Roberts, P.H. & King, E.M., 2013. On the genesis of the Earth's magnetism, Rep. Prog. Phys., 76(096801), doi:10.1088/0034-4885/76/9/096801.
- Schaeffer, N., Jault, D., Nataf, H.-C. & Fournier, A., 2017. Turbulent geodynamo simulations: a leap towards Earth's core, *Geophys. J. Int.*, 211(1), 1–29.
- Schrinner, M., Petitdemange, L., Raynaud, R. & Dormy, E., 2014. Topology and field strength in spherical, anelastic dynamo simulations, *Astr. Astrophys.*, 564, doi:10.1051/0004-6361/201322801.

- Schwaiger, T., Gastine, T. & Aubert, J., 2021. Relating force balances and flow length scales in geodynamo simulations, *Geophys. J. Int.*, 224(3), 1890–1904.
- Sheyko, A., Finlay, C., Favre, J. & Jackson, A., 2018. Scale separated low viscosity dynamos and dissipation within the Earth's core, Sci. Rep., 8(1), 12566.
- Soderlund, K.M., King, E.M. & Aurnou, J.M., 2012. The influence of magnetic fields in planetary dynamo models, *Earth Planet. Sci. Lett.*, 333-334, 9–20.
- Soward, A.M., 1977. On the finite amplitude thermal instability of a rapidly rotating fluid sphere, *Geophys. Astrophys. Fluid Dyn.*, **9**(1), 19–74.
- Stevenson, D.J., 2003. Planetary magnetic fields, *Earth Planet. Sci. Lett.*, **208**(1–2), 1–11.
- Tarduno, J.A., Cottrell, R.D., Davis, W.J., Nimmo, F. & Bono, R.K., 2015. A Hadean to Paleoarchean geodynamo recorded by single zircon crystals, *Science*, **349**(6247), 521–524.

- Taylor, J.B., 1963. The magneto-hydrodynamics of a rotating fluid and the Earth's dynamo problem, *Proc. Roy. Soc. A*, **274**, 274–283.
- Wicht, J. & Christensen, U.R., 2010. Torsional oscillations in dynamo simulations, Geophys. J. Int., 181, 1367–1380.
- Wu, C.-C. & Roberts, P.H., 2015. On magnetostrophic mean-field solutions of the geodynamo equations, *Geophys. Astrophys. Fluid Dyn.*, 109(1), 84–110.
- Yadav, R.K., Gastine, T. & Christensen, U.R., 2013a. Scaling laws in spherical shell dynamos with free-slip boundaries, *Icarus*, 225(1), 185–193.
- Yadav, R.K., Gastine, T., Christensen, U.R. & Duarte, L.D., 2013b. Consistent scaling laws in anelastic spherical shell dynamos, *Astrophys. J.*, 774(1), doi:10.1088/0004-637X/774/1/6.
- Yadav, R.K., Gastine, T. & Christensen, U.R., 2016. Approaching a realistic force balance in geodynamo simulations, *Proc. Nat. Acad. Sci.*, 113(43), 12 065–12 070.